



Feature article

Defect engineering in development of low thermal conductivity materials: A review



Meng Zhao^a, Wei Pan^{a,*}, Chunlei Wan^a, Zhixue Qu^b, Zheng Li^a, Jun Yang^a

^a State Key Lab of New Ceramics and Fine Processing, School of Materials Science and Engineering, Tsinghua University, Beijing 100084, PR China

^b College of Materials Science and Engineering, Beijing University of Technology, Beijing 100124, PR China

ARTICLE INFO

Article history:

Received 10 April 2016

Received in revised form 21 July 2016

Accepted 28 July 2016

Available online 6 August 2016

Keywords:

Thermal conductivity

Defect engineering

Phonon scattering

Thermal barrier coatings

ABSTRACT

Low thermal conductivity is the key property dominating the heat insulation ability of thermal barrier coatings (TBC). Reducing the intrinsic thermal conductivity is the major topic for developing advanced TBCs. Defect engineering has attracted much attention in seeking better TBC materials since lattice defects play a crucial role in phonon scattering and thermal conductivity reduction. Oxygen vacancies and substitutions are proven to be the most effective, while the accompanying lattice distortion is also of great importance. In this paper, recent advances of reducing the thermal conductivity of potential thermal barrier coating materials by defect engineering are comprehensively reviewed. Effects of the mass and size mismatch between the defects and the host lattice are quantitatively estimated and unconventional thermal conductivity reduction caused by the lattice distortions is also discussed. Finally, challenges and potential opportunities are briefly assessed to further minimize the thermal conductivity of TBC materials in the future.

© 2016 Elsevier Ltd. All rights reserved.

1. Introduction

Promoting the thermal efficiency and reducing emissions require gas turbine designers to further increase the operating temperature, which leads to more rigorous conditions faced by the superalloy components in the hot section, such as blades and vanes [1]. Therefore, it is urgently demanded to develop new ceramic materials with low thermal conductivity, high stability and durability at high temperature as candidates for thermal barrier coatings (TBCs) [2]. The state-of-the-art TBC material is 7 wt% yttria stabilized zirconia (7YSZ) with a low thermal conductivity about 2.5 W/m K for the fully dense bulks and less than 2 W/m K for the sprayed coatings at high temperature [3]. It may allow a 100–200 °C operating temperature increase without exceeding the limits of the superalloy components and the internal cooling system, which significantly benefits the output power and energy efficiency of the turbines [4]. Fig. 1 shows a sectional view of typical air plasma sprayed TBCs. A great deal of effort has been conducted to optimize the fabrication technologies of 7YSZ coatings during the last decade

[5–7]. Better mechanical properties and cycling lifetime have been achieved by controlling the porosity and microstructure of the coatings [8]. Yet, relatively high thermal conductivity and the t' phase degradation restrict the application of 7YSZ coatings at temperatures above 1200 °C [9,10]. In order to further improve the heat insulation ability, Ln₂Zr₂O₇-type rare earth zirconates with either pyrochlore or fluorite structure have been developed as alternative candidates of TBCs and already been applied in some J-class gas turbines (operating temperature ~1600 °C) due to their lower thermal conductivity (less than 2 W/m K for fully dense bulks at high temperature, which is 20% lower than that of 7YSZ) [11–13]. Increasing the thickness of TBCs will certainly improve the thermal insulating ability, the temperature gradient in the top-coat and retard the TGO growth. However, the increasing of thickness is strictly limited by the enhanced thermal stress produced during the thermal cycling in an oxidation environment, the thermal expansion mismatch between the top-coat and bond coat. Thicker coatings may fail to bond with bond coat alloy and may pile off the surface. Currently, the optimum thickness of TBCs for gas turbine is usually within 100–400 μm [1]. Thus, there is a consensus that even lower thermal conductivity is needed to achieve still higher gas temperature for increased energy conversion efficiency of turbines. Indeed, it has been estimated that a 50% further decrease in the thermal conductivity of TBC materials will reduce the temperature at the surface of hot section components by about 55 °C, which corresponds to the improvement of single crystal Ni-based

* Corresponding author.

E-mail addresses: zhao-m07@mails.tsinghua.edu.cn (M. Zhao), panw@mail.tsinghua.edu.cn (W. Pan), wancl@mail.tsinghua.edu.cn (C. Wan), quzhixue@bjut.edu.cn (Z. Qu), lizheng13@mails.tsinghua.edu.cn (Z. Li), yangjun13@mails.tsinghua.edu.cn (J. Yang).

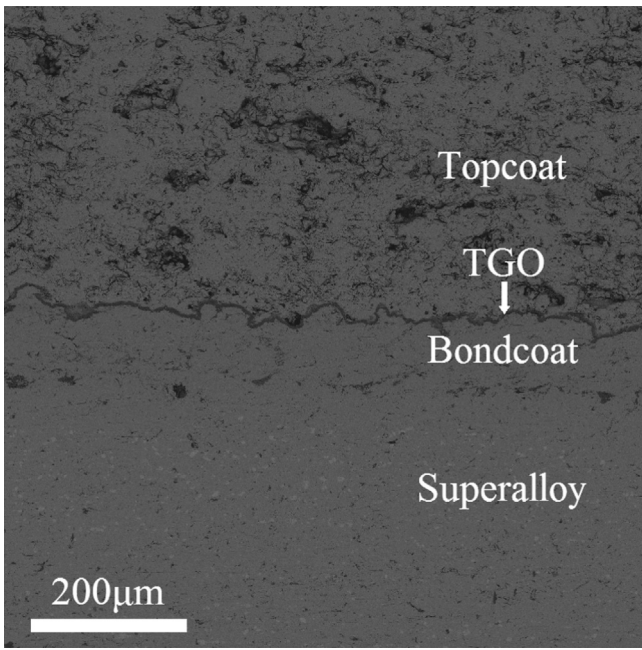


Fig. 1. A sectional view of typical air plasma sprayed thermal barrier coatings. Heat insulation is mainly provided by the ceramic topcoat. Generation of the thermally grown oxide (TGO) layer is the major failure mechanism of TBCs.

superalloy over the last 20 years [14]. Therefore, new TBC materials with even lower thermal conductivity are definitely required and a deeper fundamental understanding of the underlying heat transfer mechanisms is also necessary as the scientific guideline of future development.

As illustrated in some previous researches, some significant progress in identifying promising TBC materials has been made during the last decade. The development mainly focuses on two aspects: (1) further decrease the thermal conductivity of 7YSZ and $\text{Ln}_2\text{Zr}_2\text{O}_7$, for example designing multicomponent solid solutions based on them; (2) develop totally new material systems with low thermal conductivity, such as perovskite zirconates, rare earth hexaaluminates, orthophosphates and silicates [15–20]. In both directions, solid state heat transfer mechanism is always the theoretical foundation and defect engineering is acknowledged as the most systematic perspective and effective approach. Lattice defects, such as vacancies and substitutions, have an extremely important impact in the thermal conductivity reduction. The accompanying lattice distortion also plays a considerable role. In this paper, recent researches on the thermal conductivity of promising TBC materials have been reviewed and effects of various lattice defects on the thermal conductivity reduction are summarized and discussed in consideration of the point defect phonon scattering and lattice distortions.

2. Fundamentals of heat conduction in solid state materials

Generally, phonon propagation dominates the heat conduction in non-magnetic insulating ceramic materials [21]. However, fundamentals of understanding the phonon heat conduction in solid state materials have not been updated much from the Debye model for gas heat transfer since the 1960s due to the lack of motivation, except for some normalization on the mathematic symbols and notations. According to that, thermal conductivity of ceramic materials can be expressed as [22]:

$$\kappa = \frac{1}{3} \int_{\omega} C_V v l \quad (1)$$

where C_V is the specific heat, v is the average sound velocity and l is the phonon mean free path, which is the most important factor controlling the phonon thermal conductivity. The integration is over all the practical phonon frequencies of a certain material.

Ideal materials with defect-free lattice and perfectly harmonic vibration express infinite thermal conductivity because of the free phonon propagation and unlimited phonon mean free path. However, in real materials with defective lattice structure, phonon mean free path and thermal conductivity are limited by phonon scattering effects caused by other phonons, defects, boundaries, etc. [23]. Callaway has derived the expression of thermal conductivity on the assumption that all the phonon scattering processes can be represented by relaxation times (τ_C), as [24]:

$$\kappa = \frac{k_B}{2\pi^2 v_s} \left(\frac{k_B T}{\hbar} \right)^3 \int_0^{\theta_D/T} \tau_C(x) \frac{x^4 e^x}{(e^x - 1)^2} dx \quad (2)$$

where $x = \hbar\omega/k_B T$, k_B is the Boltzmann constant, θ_D is the Debye temperature, and v_s is the average sound velocity. Then the combined relaxation time τ_C is defined as [25]:

$$\tau_C^{-1} = \tau_p^{-1} + \tau_D^{-1} + \tau_B^{-1} \quad (3)$$

where τ_p , τ_D and τ_B respectively correspond to the relaxation time of phonon–phonon scattering, phonon–defect scattering and phonon–boundary scattering.

Generally, the phonon–boundary scattering can be omitted since the grain size is much bigger than the phonon mean free path, which is limited by the phonon–phonon and phonon–defect scatterings in bulk materials within the whole temperature range. As for the phonon–defect scattering, Klemens provided the expressions [26]:

$$\tau_D^{-1} = A\omega^4 \quad (4)$$

$$A = \frac{\Omega\Gamma}{4\pi v_s^3} \quad (5)$$

where ω is the phonon frequency and Ω is the average volume per atom. Γ is the phonon scattering coefficient, which will be further defined below. In particular, defects here refer to the point lattice defects, such as vacancies and substitutions.

In addition, the relaxation time of phonon–phonon scattering (Umklapp scattering) can be estimated as:

$$\tau_p^{-1} = S(T)\omega^2 \quad (6)$$

where $S(T)$ is proportional to the temperature ($S(T) = CT$) when $T > \theta_D$. Combining all the three aspects mentioned above, the thermal conductivity of materials can therefore be expressed as [27]:

$$\kappa = \frac{k_B}{2\pi^2 v_s \sqrt{(ACT)}} \tan^{-1} \left[\frac{k_B \theta_D}{\hbar} \left(\frac{A}{CT} \right)^{\frac{1}{2}} \right] \quad (7)$$

For “perfect crystal materials” without “intrinsic lattice defects”, the scattering coefficient Γ is approximately zero, then the thermal conductivity (κ_p) is mainly controlled by the phonon–phonon scattering:

$$\kappa_p = \frac{k_B^2 \theta_D}{2\pi^2 v_s \hbar C T} \quad (8)$$

Therefore, phonon–phonon scattering will lead to a thermal conductivity inversely proportional to the temperature, that is $\kappa_p \propto 1/T$. This is usually correct for ceramic materials without “intrinsic lattice defects”.

On the other hand, the thermal conductivity of a “real material” with lattice defects is related to that of the corresponding “perfect crystal material” by [28]:

$$\frac{\kappa}{\kappa_p} = \frac{\tan^{-1}(u)}{u} \quad (9)$$

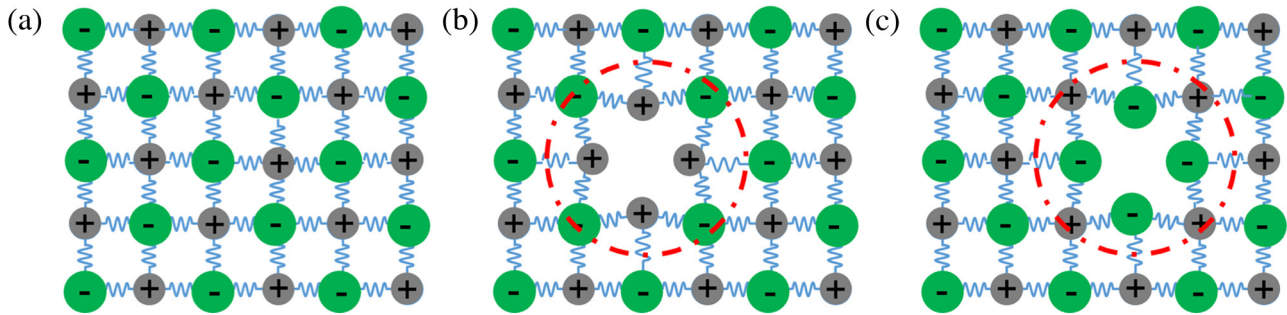


Fig. 2. Schematic drawings of: (a) perfect crystal lattice without vacancies; (b) defective lattice with anion vacancies; (c) defective lattice with cation vacancies.

where u is defined as:

$$u = \left(\frac{\pi^2 \theta_D \Omega}{h v_s^2} \kappa_p \Gamma \right)^{1/2} \quad (10)$$

Combining Eqs. (9) and (10), thermal conductivity of defective materials is approximately inversely proportional to the square root of the phonon scattering coefficient, that is $\kappa_p \propto 1/\sqrt{\Gamma}$. This usually weakens the temperature dependence of the thermal conductivity.

Based on the derivation of Klemens and Callaway, Wan, et al. have proposed a quantitative method to define the phonon scattering coefficient taking account of the effective elastic properties of the matrix material and the effective ionic radius of the defects according to the elastic continuum model [29]:

$$\Gamma_i = f_i \left\{ \left(\frac{\Delta M_i}{M} \right)^2 + 2 \left[6.4 \cdot \frac{1}{3} \gamma \frac{1+\nu}{1-\nu} \left(\frac{\Delta \delta_i}{\delta} \right)^2 \right] \right\} \quad (11)$$

where the subscript i represents a certain kind of lattice defect and f_i is the fractional concentration of them. M and δ are the average value of the atomic mass and the ionic radius on the corresponding defective crystalline site. $\Delta M_i = M - M_i$ and $\Delta \delta_i = \delta - \delta_i$, where M_i and δ_i represent the atomic mass and ionic radius of the defect. Also, γ is the Grüneisen parameter describing the average anharmonicity of the vibration within the whole lattice and ν is the Poisson ratio related to the elastic properties of the matrix material. It should be clarified that Eq. (11) is valid only when the elastic properties of the matrix material are not strongly affected by the lattice defects.

This “point defect phonon scattering model” has been widely applied to understand the effect of lattice defect on the thermal conductivity of TBC materials and it also serves as the basic guidance of the researches to reduce the thermal conductivity of TBC materials. According to the derivation above, increasing the defect concentration (f_i) will surely increase the phonon scattering coefficient and expanding the mismatch between the defect and host lattice, of both mass and size (ΔM_i and $\Delta \delta_i$), is also effective to enhance the phonon scattering and therefore reduce the thermal conductivity. Besides, some lattice defects may introduce unconventional lattice distortions, therefore leading to even lower thermal conductivity than the result of point defect phonon scattering model.

In the limit of the strongest phonon scattering at high temperature, the phonon mean free path asymptotes to a minimum value. Therefore the minimum thermal conductivity is analogous to the thermal conductivity of gases at high temperature, namely a dependence on the acoustic velocity and the inter-atomic distance. For instance, Cahill etc. have expressed the minimum thermal conductivity as [30]:

$$\kappa_{\min} = \frac{k_B}{2.48} n^{2/3} (2v_t + v_l) \quad (\text{Cahill model}) \quad (12)$$

where v_t and v_l are velocity of the transverse and longitude modes of phonon, n is the number of atoms per unit volume. An alternative expression has been given by Clarke. It is based on the same limiting condition for the phonon mean free path and the effective atomic masses, but is expressed in terms of more easily obtained physical parameters, and also gives almost the same values for simple compounds [14]:

$$\kappa_{\min} = 0.87 k_B N_A^{2/3} \frac{m^{2/3} \rho^{1/6} E^{1/2}}{M^{2/3}} \quad (\text{Clarke model}) \quad (13)$$

where k_B is the Boltzmann constant, N_A is the Avogadro number, m is the number of atoms within the unit cell, M is the average atomic mass of the unit cell and E is the Young's modulus of the material.

In this case, the minimum thermal conductivity is mainly controlled by the lattice density and elastic modulus of the materials, corresponding to the specific heat and average sound velocity in Eq. (1). Generally, heavy atomic mass and low sound velocity will lead to low thermal conductivity and this is proven valid for materials with complex lattice structure at high temperature, as concluded in some previous research [31].

3. Vacancies

As shown in Fig. 2, a vacancy is a special kind of lattice defect with a total absence of mass and a mismatch of volume on the crystalline sites as well as the surrounding chemical bonds, therefore leading to the strongest phonon scattering and lattice distortion. For vacancies on either anion or cation sub-lattice, ΔM_i and $\Delta \delta_i$ in Eq. (11) will become M_i and δ_i of the missing ion, leaving $(\Delta M_i/M)$ and $(\Delta \delta_i/\delta)$ related only to the concentration of vacancies (f_v). Therefore, a concentration increase of the vacancies will surely result in lower thermal conductivity.

3.1. Oxygen vacancies

Oxygen vacancies are the most commonly corroborated lattice defects in oxide ceramics, especially for materials with low thermal conductivity. The state-of-the-art TBC material, 7YSZ (equivalent to about $Zr_{0.92} Y_{0.08} O_{1.96}$), is a typical example. Unstabilized ZrO_2 has a monoclinic phase structure ($P2_1/c$) with a rather high thermal conductivity [32,33]. As shown in the ZrO_2 -rich region of the ZrO_2 - Y_2O_3 binary phase diagram in Fig. 3, alloying zirconia with yttria is necessary to avoid the disruptive phase transformation between the monoclinic and tetragonal, which will otherwise result in mechanical breakdown of the coatings, and also stabilizes zirconia to the metastable t' phase preferable for TBC application owing to the ferroelastic toughening mechanism [9,34]. The defect equation of the Y_2O_3 alloying in ZrO_2 can be expressed as:



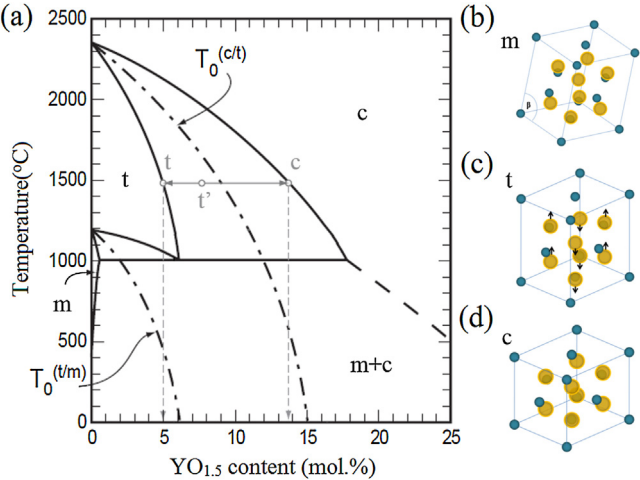


Fig. 3. The ZrO₂-rich part of the ZrO₂-Y₂O₃ binary phase diagram is given (a) and the lattice structure of the m phase (b), t phase (c) and c phase (d) of ZrO₂ [32–34].

where Y_{Zr} represents the Y^{3+} occupying the Zr^{4+} site with a negative charge and $V_0^{\bullet\bullet}$ denotes the positively charged oxygen vacancy. The substitutions of the Zr^{4+} by Y^{3+} (Y_{Zr}) certainly provide phonon scattering, yet the efficiency of them is limited by the similarity of the atomic mass and ionic radius of Y^{3+} and Zr^{4+} . Therefore, the oxygen vacancies ($V_0^{\bullet\bullet}$) which are compensations for the charge neutrality, are primarily responsible for the thermal conductivity reduction from ZrO₂ to 7YSZ. According to the stoichiometry, the concentration of oxygen vacancies in 7YSZ is only about 2%. However, the resulting reduction of the thermal conductivity is about 30%

compared with the unstabilized monoclinic ZrO₂, which is more efficient than the nearly 8% Y^{3+} substitutions.

Clearly, oxygen vacancies introduced by the aliovalent alloying in ZrO₂ are incomparably beneficial to the reduction of thermal conductivity. At moderate content of alloying, thermal conductivity of ZrO₂-Y₂O₃, ZrO₂-Gd₂O₃, ZrO₂-Yb₂O₃ binary and some ZrO₂-Y₂O₃-Ln₂O₃ ternary solid solutions decrease rapidly with the concentration increase of oxygen vacancies, which is in perfect accordance with the point defect phonon scattering model [35–40]. Similar results have also been observed in ZrO₂-Sm₂O₃ and ZrO₂-Nd₂O₃ solid solutions at temperature higher than 400 °C, although an inverse tendency is generated by the lattice disordering at ambient temperature [41–43]. However, previous research has also concluded that the thermal conductivity of ZrO₂-Ln₂O₃ solid solutions keeps decreasing with the concentration increase of the oxygen vacancies up to about 5% (corresponding to Zr_{0.8}Ln_{0.2}O_{1.9}) and then is approximately constant. This saturation behavior has been attributed to the ordering of the whole lattice and the interactions between oxygen vacancies [44].

In addition, oxide compounds with high concentration of intrinsic oxygen vacancies have been reported recently. For example, Ln₂Zr₂O₇-type rare earth zirconates with both pyrochlore (Fd $\bar{3}m$) and fluorite (Fm $3m$) structures have been developed in the pursuit of even lower thermal conductivity [45]. As reviewed by Subramanian etc., pyrochlore Ln₂Zr₂O₇ with the ordered structure can be considered as A₂B₂O₆O', where the A, B, O, O' ions and oxygen vacancies respectively occupy the crystalline Wyckoff sites 16c, 16d, 48f, 8a and 8b; while the cations are completely disordered in fluorite Ln₂Zr₂O₇ and the oxygen anions are all equivalent with one-eighth vacancy [46]. The schematic drawing of the lattice structure of pyrochlore and fluorite are shown in Fig. 4 [47]. Because of the same elemental composition and similar lattice structure, rare

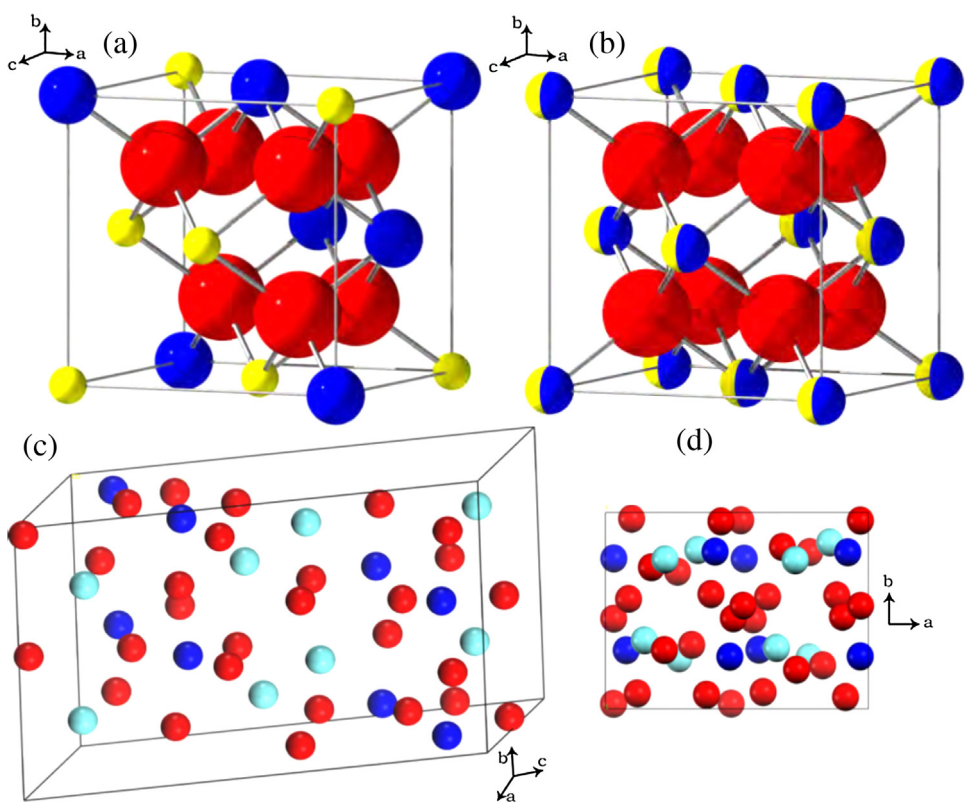


Fig. 4. Schematic drawing of the lattice structure of (a) pyrochlore; (b) defective fluorite (blue spheres are Ln^{3+} , yellow spheres are Zr^{4+} and large red spheres are O^{2-}); (c) perspective view of δ phase; (d) view down the c-axis of δ phase (light blue spheres are Ln^{3+} , dark blue spheres are Zr^{4+} and red spheres are O^{2-}) [47]. (For interpretation of the references to colour in this figure legend, the reader is referred to the web version of this article.)

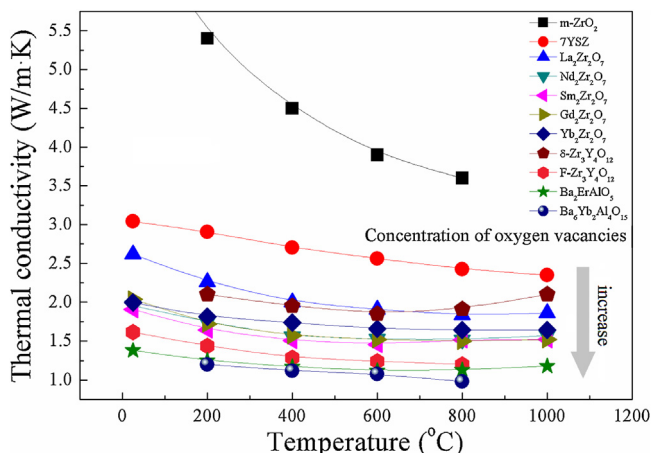


Fig. 5. Thermal conductivity of materials with oxygen vacancies. The lowest value achieved is about 1 W/m K at 800 °C.

earth zirconates also have similar mechanical properties and thermal expansion coefficient to 7YSZ. However, the concentration of intrinsic oxygen vacancies is sharply improved to about 12.5% (1/8). Therefore, low thermal conductivity can be expected in $\text{Ln}_2\text{Zr}_2\text{O}_7$ materials.

Fig. 5 shows the relation between the thermal conductivity and the temperature for several kinds of rare earth zirconates developed recently [29,48–50]. Specifically, $\text{Nd}_2\text{Zr}_2\text{O}_7$, $\text{Sm}_2\text{Zr}_2\text{O}_7$, $\text{Gd}_2\text{Zr}_2\text{O}_7$ and $\text{Yb}_2\text{Zr}_2\text{O}_7$ have almost temperature independent low thermal conductivity with little difference between each other, which indicates that the type of rare earth element and the related $\text{Ln}-\text{O}$ chemical bonds have much less effect on the thermal conductivity than the phonon scattering caused by oxygen vacancies. Their thermal conductivity is about 1.6 W/m K at 1000°. However, thermal conductivity of $\text{La}_2\text{Zr}_2\text{O}_7$ is relatively higher, about 1.9 W/m K at 1000 °C, which may be attributed to the ordered distribution of the oxygen vacancies.

Furthermore, Winter etc. have investigated the phase structure and thermal properties of Y_2O_3 -rich material $\text{Zr}_3\text{Y}_4\text{O}_{12}$ along the extension of the ZrO_2 - Y_2O_3 binary phase diagram, which may crystallize in fluorite structure or another ordered structure identified as the δ phase ($\text{R}\bar{3}$) shown in Fig. 4(c) rather than the pyrochlore structure [15,32]. With an even higher concentration of oxygen vacancies, about 14.3% (1/7), the thermal conductivity of $\text{Zr}_3\text{Y}_4\text{O}_{12}$ with the fluorite structure ($\text{F-Zr}_3\text{Y}_4\text{O}_{12}$) is only about 1.4 W/m K at 800 °C. However, as shown in Fig. 5, the thermal conductivity of $\text{Zr}_3\text{Y}_4\text{O}_{12}$ with the ordered δ phase ($\delta\text{-Zr}_3\text{Y}_4\text{O}_{12}$) is relatively higher, about 2.0 W/m K at 600 °C and a further increase at higher temperature, which is related to heat radiation [51].

Beyond the ZrO_2 - Ln_2O_3 binary solid solutions or compounds, new materials with even higher concentration of oxygen vacancies have also been designed and investigated, for example, Wan etc. have reported the thermophysical properties of $\text{Ba}_2\text{LnAlO}_5$ materials with a monoclinic phase structure ($\text{P}2_1/\text{m}$ or $\text{P}2_1$) [52]. All the $\text{Ba}_2\text{LnAlO}_5$ materials have a distinct pseudo-bcc sub cell, which shows similarity with the perovskite structure (ABO_3). Specifically, Ba^{2+} ions correspond to the A site in the perovskite structure while Ln^{3+} and Al^{3+} ions occupy the B site. One sixth of the oxygen ions are missing, resulting in an extremely high oxygen vacancy concentration of 16.7% (1/6), which is naturally conducive to phonon scattering. The thermal conductivities of $\text{Ba}_2\text{DyAlO}_5$, $\text{Ba}_2\text{ErAlO}_5$ and $\text{Ba}_2\text{YbAlO}_5$ have been reported [53]. As also shown in Fig. 5, the lowest thermal conductivity value of $\text{Ba}_2\text{DyAlO}_5$ is about 1.2 W/m K at 1000 °C, which is approaching the minimum thermal conductivity as defined in Eqs. (12) and (13). It has been indicated that not only the phonon scattering effect cutting down the phonon

Table 1
Concentration of oxygen vacancies of some oxides [13,53].

No.	Composition	f_v
0	ZrO_2	0
1	$\text{Zr}_{0.92}\text{Y}_{0.08}\text{O}_{1.96}$ (7YSZ)	2%
2	$\text{La}_2\text{Zr}_2\text{O}_7$	12.5%
3	$\text{Nd}_2\text{Zr}_2\text{O}_7$	12.5%
4	$\text{Sm}_2\text{Zr}_2\text{O}_7$	12.5%
5	$\text{Gd}_2\text{Zr}_2\text{O}_7$	12.5%
6	$\text{Yb}_2\text{Zr}_2\text{O}_7$	12.5%
7	$\text{Zr}_3\text{Y}_4\text{O}_{12}$	14.3%
8	$\text{Ba}_2\text{DyAlO}_5$	16.7%
9	$\text{Ba}_2\text{ErAlO}_5$	16.7%
10	$\text{Ba}_2\text{YbAlO}_5$	16.7%
11	$\text{Ba}_6\text{Gd}_2\text{Al}_4\text{O}_{15}$	16.7%
12	$\text{Ba}_6\text{Dy}_2\text{Al}_4\text{O}_{15}$	16.7%
13	$\text{Ba}_6\text{Er}_2\text{Al}_4\text{O}_{15}$	16.7%
14	$\text{Ba}_6\text{Yb}_2\text{Al}_4\text{O}_{15}$	16.7%

mean free path, but also the reduced average sound velocity is of benefit to their ultralow thermal conductivity. Shortly afterwards, $\text{Ba}_6\text{Ln}_2\text{Al}_4\text{O}_{15}$ materials with a similar but much more complex lattice structure ($\text{P}2_1/\text{m}$ or $\text{P}2_1$) have also been developed by Feng etc. [54]. In principle, they are tripled from $\text{Ba}_2\text{LnAlO}_5$ with a substitution of Ln^{3+} by Al^{3+} and therefore have the same concentration of oxygen vacancies. The thermal conductivities of $\text{Ba}_6\text{Gd}_2\text{Al}_4\text{O}_{15}$, $\text{Ba}_6\text{Dy}_2\text{Al}_4\text{O}_{15}$, $\text{Ba}_6\text{Er}_2\text{Al}_4\text{O}_{15}$ and $\text{Ba}_6\text{Yb}_2\text{Al}_4\text{O}_{15}$ are also shown in Fig. 5. The thermal conductivity is less than 1.4 W/m K for all the materials within the temperature range of 300 °C–800 °C and the lowest value at 800 °C is about 1.0 W/m K of $\text{Ba}_6\text{Yb}_2\text{Al}_4\text{O}_{15}$. To the best of our knowledge, $\text{Ba}_2\text{LnAlO}_5$ and $\text{Ba}_6\text{Ln}_2\text{Al}_4\text{O}_{15}$ materials have the highest oxygen vacancy concentration and also the lowest thermal conductivity of all the refractory oxide ceramic materials for high temperature applications known by now.

As listed in Table 1, from ZrO_2 to 7YSZ, from $\text{Ln}_2\text{Zr}_2\text{O}_7$ to $\text{Zr}_3\text{Ln}_4\text{O}_{12}$ and then to $\text{Ba}_2\text{LnAlO}_5$ and $\text{Ba}_6\text{Ln}_2\text{Al}_4\text{O}_{15}$, their design perspective has always been increasing the concentration of oxygen vacancies. Their thermal conductivity generally decreases with increasing concentration of oxygen vacancies within the whole temperature range as summarized in Fig. 6, which is in accordance with the point defect phonon scattering model, except for a slight thermal conductivity fluctuation of materials with the same concentration of oxygen vacancies due to the ordered distribution of the vacancies. The lowest thermal conductivity achieved by this vacancy strategy is about 1 W/m K at high temperature, which is approaching to the theoretical minimum.

3.2. Cation vacancies

Different from oxygen vacancies of the anion sub-lattice, cation vacancies are relatively rare in ceramic oxides with simple lattice structures, such as pyrochlore or fluorite. The possible reason is that without the chemical bonds centered on the cations, the relatively big anions will be too close to hold the lattice structure against the repulsions. A special case is the apatite gadolinium calcium silicates $\text{Gd}_{8+x}\text{Ca}_{2+y}(\text{SiO}_4)_6\text{O}_{2+3x/2+y}$ investigated by Qu etc [55]. As shown in Fig. 7, the stoichiometric material of this series, $\text{Gd}_8\text{Ca}_2(\text{SiO}_4)_6\text{O}_2$, possesses a hexagonal phase structure ($\text{P}6_3/\text{m}$) and the general formula of them can be represented as $\text{A}_6\text{A}'_4(\text{SiO}_4)_6\text{O}_{2+\delta}$, where the two kinds of A site can be occupied by rare earth ions, alkaline earth ions or both kinds of vacancies [56]. The oxygen stoichiometry parameter δ varies with the net valence of the A site, over the range of -2 to 1. Owing to the complex structure and flexible chemical composition, both oxygen and cation vacancies can be created and the concentration is controlled by systematically adjusting the relative proportions of alkaline earth and rare earth cations. Therefore based on these materials, the effect of cation

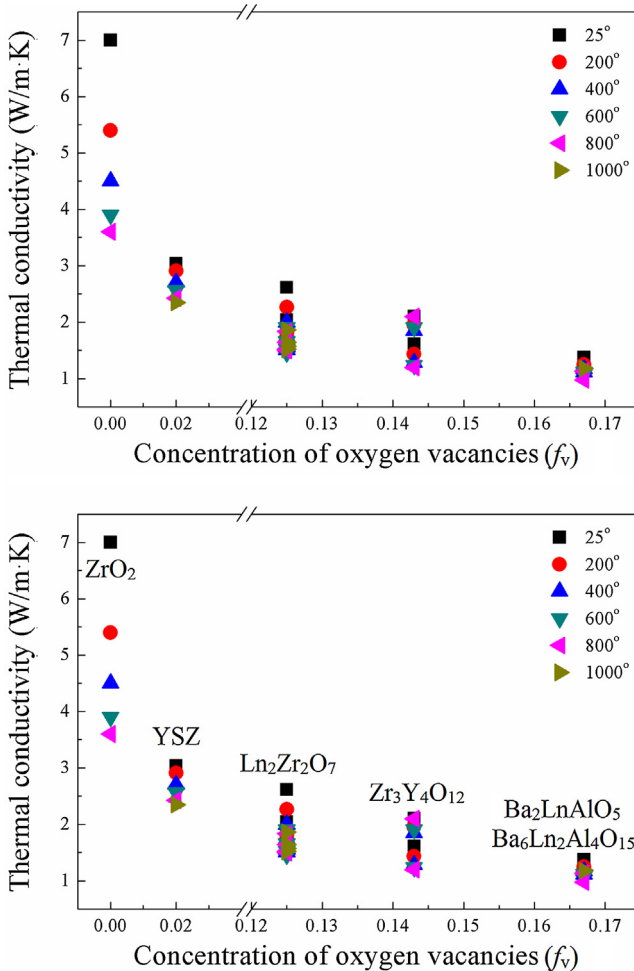


Fig. 6. Thermal conductivity decreases rapidly with the concentration increase of oxygen vacancies within the whole temperature range.

vacancies on the thermal conductivity can be investigated and compared with that of oxygen vacancies. The chemical composition, structural information and the dominating lattice defect of the materials in consideration are all listed in **Table 2** [56].

Specifically, for materials with positive x and negative y , cation vacancies are the dominating lattice defects, except for $\text{Gd}_{10}(\text{SiO}_4)_6\text{O}_3$ with oxygen interstitials. As shown in **Fig. 8**, their

Table 2

Chemical composition, structural information and the dominating lattice defect of the $\text{Gd}_{8+x}\text{Ca}_{2+y}(\text{SiO}_4)_6\text{O}_{2+3x/2+y}$ materials [56].

No.	Composition	x	y	Defect type	Defects per unit cell
1	$\text{Gd}_6\text{Ca}_4(\text{SiO}_4)_6\text{O}$	-2	2	Oxygen vacancy	1
2	$\text{Gd}_7\text{Ca}_3(\text{SiO}_4)_6\text{O}_{1.5}$	-1	1	Oxygen vacancy	1/2
3	$\text{Gd}_8\text{Ca}_2(\text{SiO}_4)_6\text{O}_2$	0	0	None	0
4	$\text{Gd}_{8.33}\text{Ca}_{1.5}(\text{SiO}_4)_6\text{O}_{2}$	1/3	-1/2	Cation vacancy	1/6
5	$\text{Gd}_{8.66}\text{Ca}(\text{SiO}_4)_6\text{O}_2$	2/3	-1	Cation vacancy	1/3
6	$\text{Gd}_{9.33}(\text{SiO}_4)_6\text{O}_2$	4/5	-2	Cation vacancy	2/3
7	$\text{Gd}_{10}(\text{SiO}_4)_6\text{O}_3$	2	-2	Oxygen interstitial	1

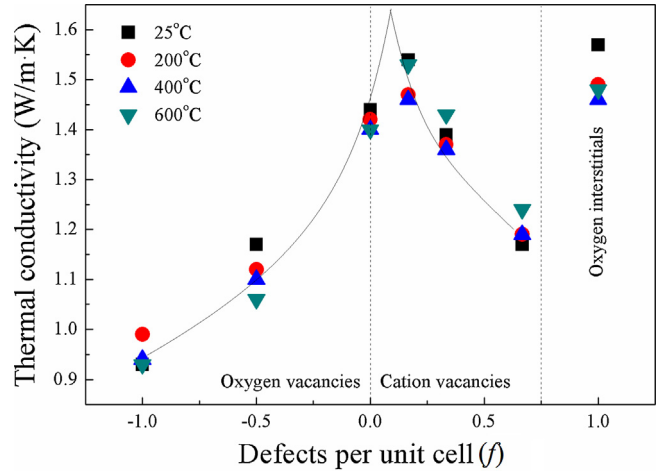


Fig. 8. Both oxygen and cation vacancies can efficiently reduce the thermal conductivity of materials. However, effect of oxygen vacancies is strong than cation vacancies at the same concentration. It should be clarified that the highest thermal conductivity doesn't belong to the stoichiometric material because of the impurity phases. Besides, oxygen interstitials may slightly increase the thermal conductivity.

thermal conductivity decreases with increasing concentration of cation vacancies, which also coincides with the point defect phonon scattering model. On the other hand, when x is negative and y is positive, the dominating lattice defects become oxygen vacancies. The thermal conductivity of these materials is even lower than those with cation vacancies, indicating that the phonon scattering of oxygen vacancies is stronger than that of cation vacancies. Since effects of both kinds of vacancies obey the point defect phonon scattering model, the lower thermal conductivity then represents the greater phonon scattering coefficient, which is probably caused by the relatively bigger ionic radius of anions than cations.

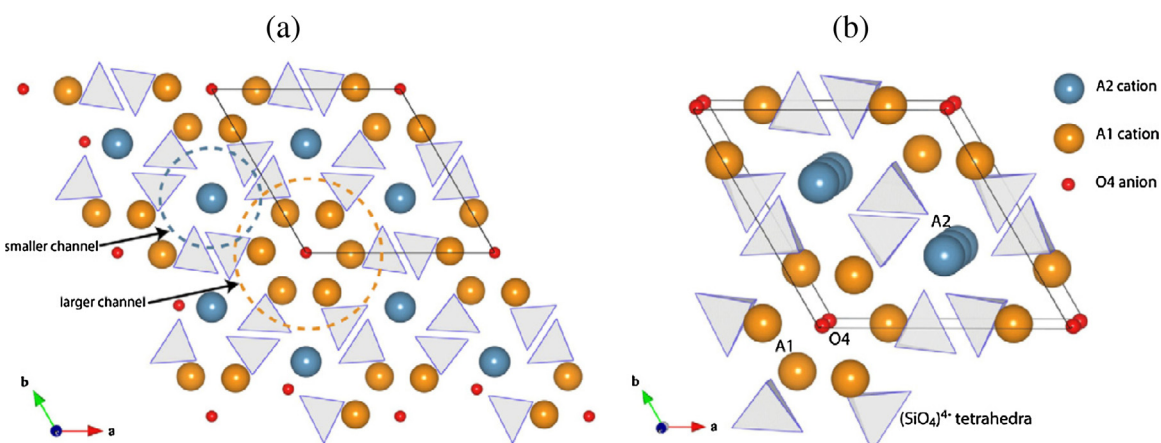


Fig. 7. Schematic drawing of the lattice structure of $\text{Gd}_{8+x}\text{Ca}_{2+y}(\text{SiO}_4)_6\text{O}_{2+3x/2+y}$ materials (a) view along the [001] axis; (b) the location of the two kinds of cation sites, A1 and A2, as well as the oxygen site O4. (No vacancies or interstitials are shown in the figure) [55,56].

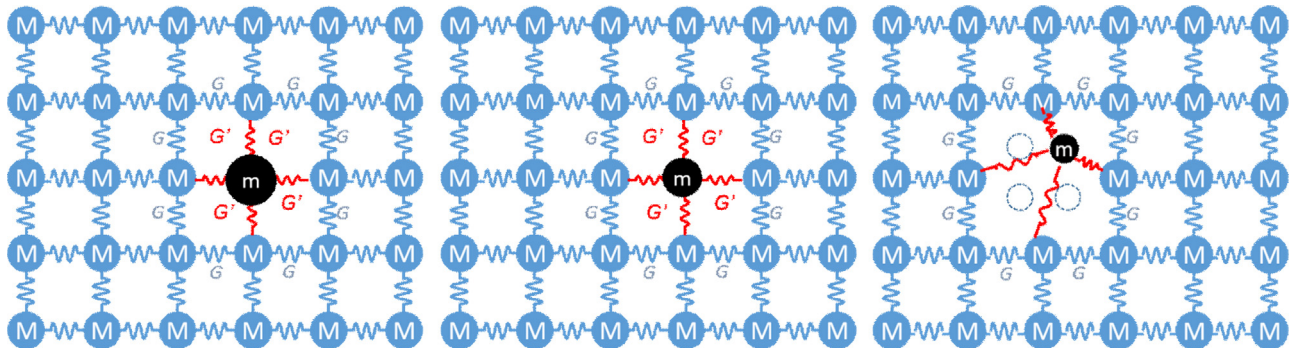


Fig. 9. Schematic drawings of the lattice with (a) substitutions with bigger size; (b) substitutions with similar size; (c) substitutions with smaller size providing the “rattling effect”.

Table 3

Atomic mass and ionic radius of elements mentioned in this paper. The two kinds of ionic radius of quadrivalent ions respectively correspond to the VI and VIII coordination states (VI/VIII). And the ionic radius of O^{2-} is calculated from the lattice parameters [64].

Element	Atomic mass	Ionic radius (pm)	Element	Atomic mass	Ionic radius (pm)
La^{3+}	138.9	116	Zr^{4+}	91.2	72/84
Nd^{3+}	144.2	110.5	Ti^{4+}	47.9	60/74
Sm^{3+}	150.4	108	Hf^{4+}	178.5	71/83
Gd^{3+}	157.3	106.5	Sn^{4+}	118.7	69/81
Er^{3+}	167.3	100.5	Ce^{4+}	140.1	87/97
Yb^{3+}	173.0	98.5	Th^{4+}	232.03	94/105
Y^{3+}	88.9	90/102	O^{2-}	16.0	137

In summary, the thermal conductivity of ceramic materials as potential TBC candidates generally decreases with the concentration increase of vacancies due to the phonon scattering, either anions or cations. However, the effect of vacancies may be slightly depressed by the ordered distribution of them at high concentration, leading to a small deviation from the expected result of the point defect phonon scattering model.

4. Substitutions

According to Eq. (11), substitutions may be less efficient in phonon scattering than vacancies due to the relatively smaller mismatch of both mass and size. However, the concentration of oxygen vacancies can hardly be further improved without destroying the phase stability. Besides, oxygen vacancies may enhance the oxygen conductivity, leading to an acceleration of the TGO growth, which is the major failure mechanism of TBCs [57]. On the other hand, equivalent substitutions can reduce the phonon mean free path without changing the intrinsic concentration of vacancies and the concentration of them can be much higher than vacancies because of the better chemical and structural compatibility. Besides, lattice distortions caused by the substitutions are also effective in reducing the thermal conductivity. Fig. 9 schematically shows the structure of lattice with bigger, similar or smaller sized substitutions. According to this substitution strategy, a lot of multicomponent materials based on 7YSZ or $Ln_2Zr_2O_7$ have been developed during the last decade and much lower thermal conductivity have already been achieved.

4.1. Substitutions in 7YSZ

In spite of ZrO_2 ceramics stabilized by the same molar content of Y^{3+} , Gd^{3+} and Yb^{3+} having the same concentration of oxygen vacancies, their thermal conductivities are quite different due to the different values of ΔM_i and $\Delta \delta_i$ between the dopant ions and Zr^{4+} [58,59]. As shown in Fig. 10, Gd^{3+} and Yb^{3+} dopants are much more efficient in the thermal conductivity reduction than Y^{3+} . Similarly, quadrivalent dopants substituting for Zr^{4+} (M_{Zr}) are also promising

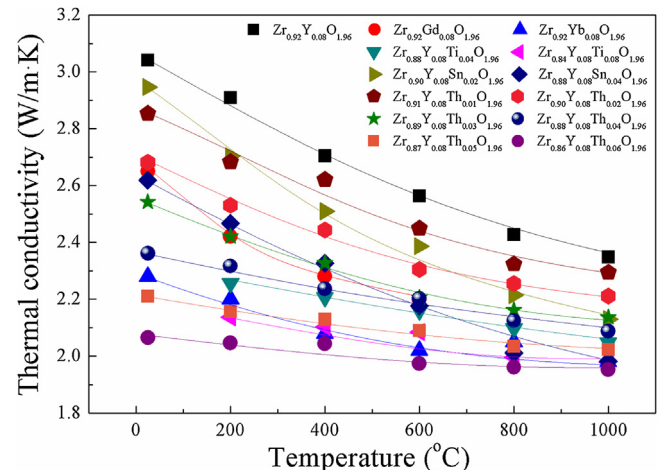


Fig. 10. Thermal conductivity of equivalent substituted 7YSZ materials.

in reducing the thermal conductivity of 7YSZ without changing the concentration of oxygen vacancies:



Previous research has reported the phase structure and thermal properties of 7YSZ with Ti^{4+} , Sn^{4+} and Th^{4+} substitutions [60–62]. According to the atomic masses listed in Table 3, Th^{4+} substitutions may provide the strongest phonon scattering due to the extremely heavy atomic mass, while Ti^{4+} substitutions may take the second place and then Sn^{4+} substitutions, which is $(\Delta M/M)_{Th4+} > (\Delta M/M)_{Ti4+} > (\Delta M/M)_{Sn4+}$. On the other hand, it has also been revealed that Th^{4+} substitutions have little influence on the lattice structure of 7YSZ, except for the smooth variation of the lattice parameter with the ionic radius of substitutions. However, strong lattice distortion is observed in Ti^{4+} and Sn^{4+} substituted materials owing to the much smaller ionic radius of Ti^{4+} and the covalent $Sn-O$ bonds [61,63]. The oxygen vacancies are also redistributed, which is caused by the interaction between the vacancies

Table 4

Phonon scattering coefficient caused by the quadrivalent substitutions in 7YSZ. Effects of Y^{3+} substitutions and the oxygen vacancies are considered as the baseline [61–63].

No.	Composition	f_i	$\Delta M/M$	$\Delta \delta/\delta$	Γ
1	Zr _{0.92} Y _{0.08} O _{1.96} (7YSZ)	0	/	/	0
2	Zr _{0.88} Y _{0.08} Ti _{0.04} O _{1.96} (4TiYSZ)	0.04	0.4850	0.2363 ^a	0.1702
3	Zr _{0.84} Y _{0.08} Ti _{0.08} O _{1.96} (8TiYSZ)	0.08	0.4946	0.2825 ^a	0.3472
4	Zr _{0.90} Y _{0.08} Sn _{0.02} O _{1.96} (2SnYSZ)	0.02	0.3003	0.2825 ^a	0.1167
5	Zr _{0.88} Y _{0.08} Sn _{0.04} O _{1.96} (4SnYSZ)	0.04	0.2985	0.2841 ^a	0.2360
6	Zr _{0.91} Y _{0.08} Th _{0.01} O _{1.96} (1ThYSZ)	0.01	1.5234	0.2452	0.0665
7	Zr _{0.90} Y _{0.08} Th _{0.02} O _{1.96} (2ThYSZ)	0.02	1.5006	0.2446	0.1312
8	Zr _{0.89} Y _{0.08} Th _{0.03} O _{1.96} (3ThYSZ)	0.03	1.4784	0.2440	0.1942
9	Zr _{0.88} Y _{0.08} Th _{0.04} O _{1.96} (4ThYSZ)	0.04	1.4568	0.2434	0.2555
10	Zr _{0.87} Y _{0.08} Th _{0.05} O _{1.96} (5ThYSZ)	0.05	1.4359	0.2428	0.3153
11	Zr _{0.86} Y _{0.08} Th _{0.06} O _{1.96} (6ThYSZ)	0.06	1.4156	0.2422	0.3737

^a For Ti⁴⁺ and Sn⁴⁺ substitutions, the effective ionic radius is considered as the value at the corresponding coordination situation, rather than the value shown in Table 3.

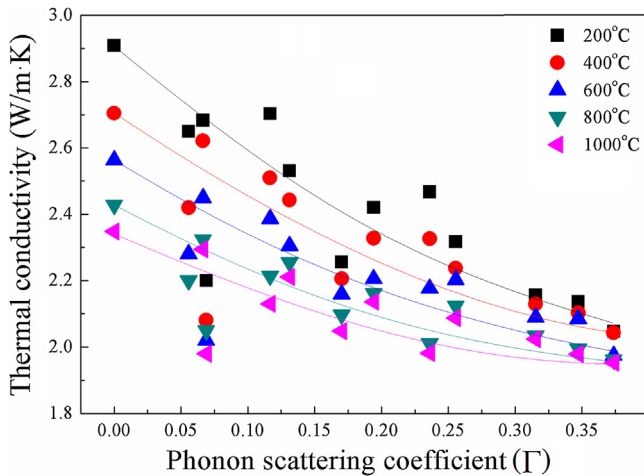


Fig. 11. For all the equivalent substituted 7YSZ materials, the thermal conductivity generally decreases with the increase of the phonon scattering coefficient. The lines are visual guides.

and substitutions. Different from the eight-fold coordinated Zr⁴⁺ in the host lattice, six-fold coordinated Ti⁴⁺ and four-fold coordinated Sn⁴⁺ are observed by structure analysis, which may have unexpected effects on the thermal conductivity.

As summarized in Fig. 10, all of the quadrivalent substitutions effectively reduce the thermal conductivity of 7YSZ and the efficiency strongly depends on the type and concentration of them. According to the point defect phonon scattering model, the effect of the substitutions on the thermal conductivity reduction can be quantitatively estimated by the phonon scattering coefficient. $\Delta M/M$ and $\Delta \delta/\delta$ for materials with Ti⁴⁺, Sn⁴⁺ and Th⁴⁺ substituents are listed in Table 4 together with the concentration of them (f_i) and then the phonon scattering coefficients (Γ) are calculated using Eq. (11) [64]. In order to estimate the effect of lattice distortions caused by the substitutions, the ionic radii of Ti⁴⁺ and Sn⁴⁺ were counted as the values of the practical coordination situations. The phonon scattering coefficients comply with the sequence of $\Gamma_{\text{Th}^{4+}} > \Gamma_{\text{Sn}^{4+}} > \Gamma_{\text{Ti}^{4+}}$ at the same substituting concentration. It should be noticed that the effects of the substitutions on the lattice vibration anharmonicity and elastic properties are neglected due to the lack of data, so the Grüneisen parameter and Poisson ratio are considered as constant for all the materials in the calculation, which will result in some uncertainty in the results.

As summarized in Fig. 11, within the temperature range of 200 °C to 1000 °C, the thermal conductivity of all the quadrivalent substituted 7YSZ materials generally decreases with the phonon

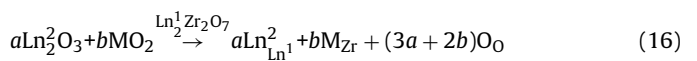
scattering coefficient increase, which just corresponds to the point defect phonon scattering model. Thermal conductivities of GdSZ and YbSZ are also given as comparisons and the relatively low result of YbSZ is probably attributed to the lattice tetragonal distortion, which is difficult to quantitatively estimate.

Apart from the equivalent substitutions with constant concentration of oxygen vacancies, a special example is that Shen etc. have studied equimolar Y_2O_3 and Ta_2O_5 co-doped ZrO_2 materials without oxygen vacancies [65]. Unlike the randomly distributed point defects, Y^{3+} and Ta^{5+} ions spontaneously form defect pairs substituting two Zr^{4+} ions due to the considerable interaction between them. A temperature independent thermal conductivity of about 1.9 W/m K is obtained for $Zr_{0.62}(YTa)_{0.19}O_2$ material from ambient temperature to 900 °C, which is lower than all of the substituted 7YSZ materials listed in Table 4. The reduction of thermal conductivity is attributed only to the phonon scattering caused by the substitutions since oxygen vacancies are totally absent in these materials. Furthermore, another 20% reduction of the thermal conductivity has been achieved by alloying with Yb_2O_3 instead of Y_2O_3 due to the bigger mass mismatch. Similar results have also been reported in ZrO_2 - Ln_2O_3 - Nb_2O_5 ternary solid solutions [66]. It needs to be mentioned that, the thermal conductivity reduction of these materials still obeys the point defect phonon scattering model, although the interactions between the point defects cannot be ignored.

Better than the defect pairs of $[Y^{3+}-Ta^{5+}]$, some special defect clusters consisting of two or more substitutions may provide stronger phonon scattering than the sum of their individual contributions and therefore lead to lower thermal conductivities than the point defect phonon scattering model suggests. The most typical example is given by the multiply doped ZrO_2 materials ZrO_2 - Y_2O_3 - Nd_2O_3 - (Gd_2O_3, Sm_2O_3) - Yb_2O_3 - (Sc_2O_3) developed by scientists from NASA [67]. The composition is designed in consideration of the interatomic and chemical potentials, lattice elastic strain energy, polarization and electro-neutrality within the whole lattice. Consisting of several point lattice defects, defect clusters with appropriate sizes lead to strong lattice distortion and provide extremely effective phonon scattering. The thermal conductivity of these multicomponent materials can be reduced towards the theoretical minimum. Besides, the lattice defect clusters can also attenuate the radiation thermal conductivity at high temperature and the cycling performance and anti-sintering property are improved as well. As a comprehensive result, these multicomponent materials with complex chemical composition and defective structure are the best optimizations of 7YSZ to date. It also reveals the potential of systematically designed defect clusters in reducing the thermal conductivity, which provides an alternative perspective for us to develop new materials with low thermal conductivity.

4.2. Substitutions in $Ln_2Zr_2O_7$

As mentioned above, $Ln_2Zr_2O_7$ compounds with high intrinsic concentrations of oxygen vacancies have attracted much attention as promising TBC materials due to their low thermal conductivity, high phase stability and relative good comprehensive mechanical performance at high temperature. Recently, substitutions have also been introduced into $Ln_2Zr_2O_7$ materials to pursue even lower thermal conductivity. Ternary and quaternary solid solutions based on $Ln_2Zr_2O_7$ have been developed as $Ln^{1-x}L^n^2_xZr_2O_7$, $Ln_2Zr_{2-x}M_xO_7$ or $Ln^{1-x}L^n^2_xZr_{2-x}M_xO_7$, where Ln^1 or Ln^2 are different kinds of rare earth elements and M is quadrivalent elements such as Ti, Hf, Sn and Ce. The defect equation can be expressed as:



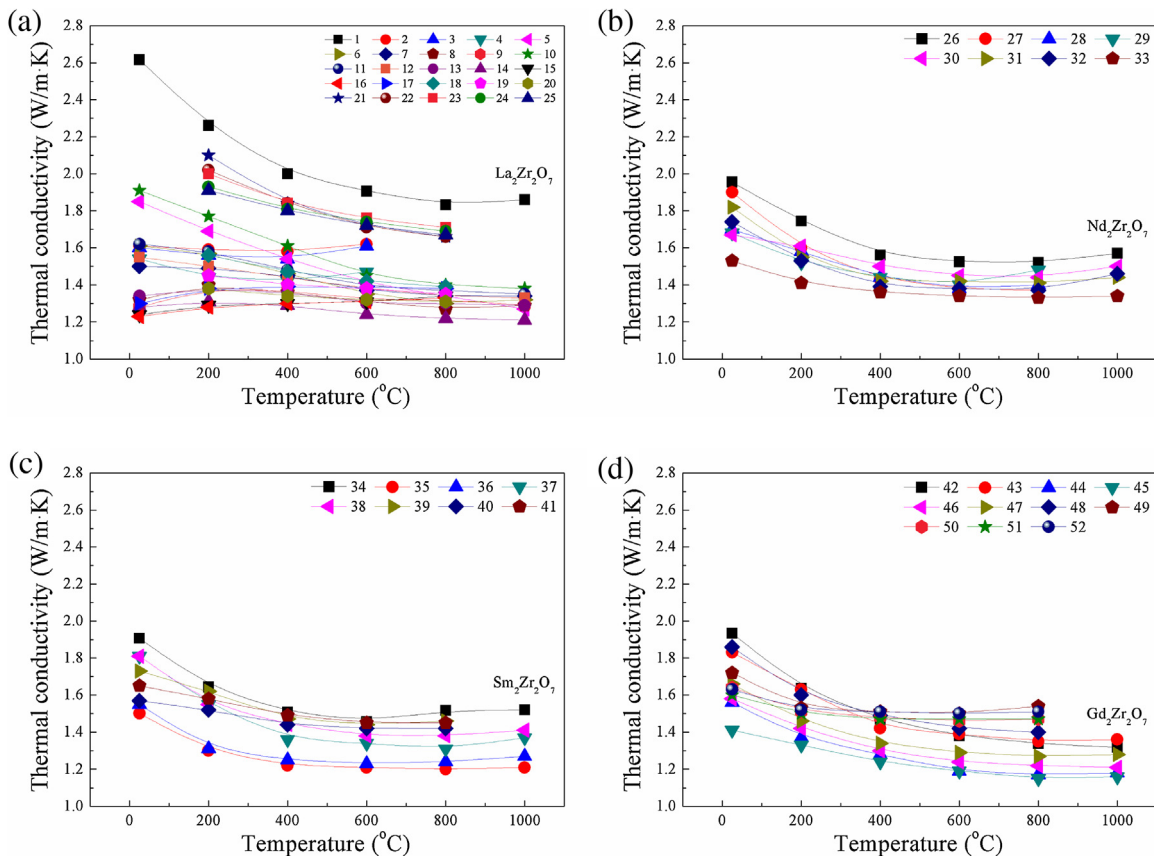


Fig. 12. Thermal conductivity of equivalent substituted materials based on (a) $\text{La}_2\text{Zr}_2\text{O}_7$; (b) $\text{Nd}_2\text{Zr}_2\text{O}_7$; (c) $\text{Sm}_2\text{Zr}_2\text{O}_7$; (d) $\text{Gd}_2\text{Zr}_2\text{O}_7$.

where Ln^1 and Ln^2 are different rare earth elements and M represents a quadrivalent element. Clearly, Substitutions in these materials are all equivalent ($\text{Ln}^2_{\text{Ln}^1}$ or M_{Zr}), therefore no more oxygen vacancies are generated and the lattice distortion is also caused by the substitution only.

Some multicomponent rare earth zirconates investigated in previous researches are summarized and divided into four groups based on the host lattice of $\text{La}_2\text{Zr}_2\text{O}_7$, $\text{Nd}_2\text{Zr}_2\text{O}_7$, $\text{Sm}_2\text{Zr}_2\text{O}_7$ and $\text{Gd}_2\text{Zr}_2\text{O}_7$ in Table 5 [29,48–50,68–75]. Their thermal conductivities are shown in Fig. 12. Clearly, the thermal conductivity are effectively reduced by the substitutions, especially for the $\text{La}_2\text{Zr}_2\text{O}_7$ -based materials. The lowest value is about 1.2 W/m·K at 1000 °C, which is about 40% lower than that of $\text{La}_2\text{Zr}_2\text{O}_7$.

The phonon scattering coefficients of the substituted $\text{Ln}_2\text{Zr}_2\text{O}_7$ materials have been calculated according to Eq. (11) in a similar manner to the substituted 7YSZ ceramics and the results are listed in Table 5. For the co-substituted materials, the phonon scattering coefficient is simply counted as the sum of each kind of substitution. As summarized in Fig. 13, the thermal conductivities of the majority of the substituted $\text{Ln}_2\text{Zr}_2\text{O}_7$ materials at 200 °C decrease with increasing phonon scattering coefficient, which indicates that the effect of the substitutions on the thermal conductivity of $\text{Ln}_2\text{Zr}_2\text{O}_7$ materials is also basically in accord with the point defect phonon scattering model, although the elastic property variations of the matrix materials due to the substitutions bring about larger uncertainties of the data than the substituted 7YSZ materials.

However, unexpectedly low thermal conductivities are also obtained at the bottom left corner, corresponding to materials with rather small phonon scattering coefficients, which is attributed to some unconventional lattice distortions in previous research. For example, in $(\text{Nd}_{1-x}\text{Yb}_x)_2\text{Zr}_2\text{O}_7$, $(\text{Sm}_{1-x}\text{Yb}_x)_2\text{Zr}_2\text{O}_7$ and $(\text{Gd}_{1-x}\text{Yb}_x)_2\text{Zr}_2\text{O}_7$ series, materials near the critical point of

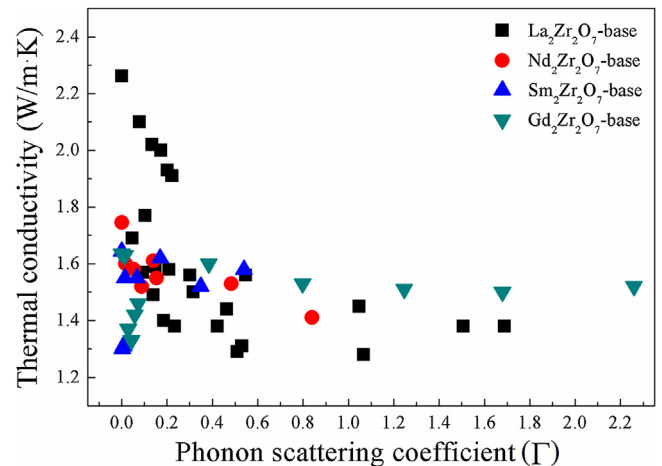


Fig. 13. For most of the substituted $\text{Ln}_2\text{Zr}_2\text{O}_7$ materials, thermal conductivity decreases with the increase of the phonon scattering coefficient, except for those with unconventional lattice distortions at the left bottom corner.

the order-disorder phase transformation between pyrochlore and fluorite structures have much lower thermal conductivities than suggested by the point defect phonon scattering model, which is mainly caused by the lattice distortion and phonon mode softening [50,69,75]. Similar phenomena are also observed in some quaternary solid solutions [76]. Broadening of the Raman active modes confirms this hypothesis and the full width at half maximum (FWHM) of the Raman peaks is applied as a semi-quantitative estimation [19]. However, it is certainly inappropriate for materials without Raman activity. Besides, a so-called “rattling” phenomenon has been reported in $(\text{La}_{1-x}\text{Yb}_x)_2\text{Zr}_2\text{O}_7$ materials [72]. As schemat-

Table 5

Phonon scattering coefficient caused by the equivalent substitutions in rare earth zirconates [29,48–50].

No.	Composition	f_i	$\Delta M/M$	$\Delta\delta/\delta$	Γ
1	$\text{La}_2\text{Zr}_2\text{O}_7$	0	/	/	0
2	$(\text{La}_{5/6}\text{Gd}_{1/6})_2\text{Zr}_2\text{O}_7$	1/6	0.1296	0.0830	0.1466
3	$(\text{La}_{2/3}\text{Gd}_{1/3})_2\text{Zr}_2\text{O}_7$	1/3	0.1269	0.0842	0.3005
4	$(\text{La}_{1/2}\text{Gd}_{1/2})_2\text{Zr}_2\text{O}_7$	1/2	0.1242	0.0854	0.4635
5	$(\text{La}_{0.98}\text{Er}_{0.02})_2\text{Zr}_2\text{O}_7$	0.02	0.2036	0.1340	0.0457
6	$(\text{La}_{0.96}\text{Er}_{0.04})_2\text{Zr}_2\text{O}_7$	0.04	0.2028	0.1343	0.0918
7	$(\text{La}_{0.94}\text{Er}_{0.06})_2\text{Zr}_2\text{O}_7$	0.06	0.2020	0.1347	0.1385
8	$(\text{La}_{0.92}\text{Er}_{0.08})_2\text{Zr}_2\text{O}_7$	0.08	0.2012	0.1351	0.1858
9	$(\text{La}_{0.90}\text{Er}_{0.10})_2\text{Zr}_2\text{O}_7$	0.10	0.2004	0.1354	0.2332
10	$(\text{La}_{0.98}\text{Er}_{0.01}\text{Yb}_{0.01})_2\text{Zr}_2\text{O}_7$	0.01+0.01	0.2036+0.2444	0.1340+0.1513	0.0521
11	$(\text{La}_{0.96}\text{Er}_{0.02}\text{Yb}_{0.02})_2\text{Zr}_2\text{O}_7$	0.02+0.02	0.2026+0.2433	0.1344+0.1517	0.1046
12	$(\text{La}_{0.94}\text{Er}_{0.03}\text{Yb}_{0.03})_2\text{Zr}_2\text{O}_7$	0.03+0.03	0.2017+0.2422	0.1348+0.1522	0.1579
13	$(\text{La}_{0.92}\text{Er}_{0.04}\text{Yb}_{0.04})_2\text{Zr}_2\text{O}_7$	0.04+0.04	0.2009+0.2412	0.1352+0.1526	0.2116
14	$(\text{La}_{0.90}\text{Er}_{0.05}\text{Yb}_{0.05})_2\text{Zr}_2\text{O}_7$	0.05+0.05	0.2000+0.2401	0.1355+0.1530	0.2649
15	$(\text{La}_{5/6}\text{Yb}_{1/6})_2\text{Zr}_2\text{O}_7$	1/6	0.2358	0.1548	0.5095
16	$(\text{La}_{2/3}\text{Yb}_{1/3})_2\text{Zr}_2\text{O}_7$	1/3	0.2270	0.1588	1.0668
17	$(\text{La}_{1/2}\text{Yb}_{1/2})_2\text{Zr}_2\text{O}_7$	1/2	0.2187	0.1632	1.6886
18	$\text{La}_2(\text{Zr}_{0.9}\text{Ce}_{0.1})_2\text{O}_7$	0.1	0.5089	0.2041	0.5466
19	$\text{La}_2(\text{Zr}_{0.8}\text{Ce}_{0.2})_2\text{O}_7$	0.2	0.4843	0.2000	1.0469
20	$\text{La}_2(\text{Zr}_{0.7}\text{Ce}_{0.3})_2\text{O}_7$	0.3	0.4619	0.1961	1.5061
21	$\text{La}_2(\text{Zr}_{0.9}\text{Hf}_{0.1})_2\text{O}_7$	0.1	0.8736	0.0139	0.0787
22	$\text{La}_2(\text{Zr}_{0.8}\text{Hf}_{0.2})_2\text{O}_7$	0.2	0.8034	0.0139	0.1339
23	$\text{La}_2(\text{Zr}_{0.7}\text{Hf}_{0.3})_2\text{O}_7$	0.3	0.7437	0.0139	0.1732
24	$\text{La}_2(\text{Zr}_{0.6}\text{Hf}_{0.4})_2\text{O}_7$	0.4	0.6922	0.0140	0.2015
25	$\text{La}_2(\text{Zr}_{0.5}\text{Hf}_{0.5})_2\text{O}_7$	0.5	0.6474	0.0140	0.2218
26	$\text{Nd}_2\text{Zr}_2\text{O}_7$	0	/	/	0
27	$(\text{Nd}_{0.9}\text{Gd}_{0.1})_2\text{Zr}_2\text{O}_7$	0.1	0.0900	0.0363	0.0173
28	$(\text{Nd}_{0.7}\text{Gd}_{0.3})_2\text{Zr}_2\text{O}_7$	0.3	0.0884	0.0366	0.0526
29	$(\text{Nd}_{0.5}\text{Gd}_{0.5})_2\text{Zr}_2\text{O}_7$	0.5	0.0869	0.0369	0.0889
30	$(\text{Nd}_{0.9}\text{Gd}_{0.05}\text{Yb}_{0.05})_2\text{Zr}_2\text{O}_7$	0.05+0.05	0.0896+0.1969	0.0373+0.1102	0.1401
31	$(\text{Nd}_{0.9}\text{Yb}_{0.1})_2\text{Zr}_2\text{O}_7$	0.1	0.1958	0.1098	0.1545
32	$(\text{Nd}_{0.7}\text{Yb}_{0.3})_2\text{Zr}_2\text{O}_7$	0.3	0.1884	0.1123	0.4836
33	$(\text{Nd}_{0.5}\text{Yb}_{0.5})_2\text{Zr}_2\text{O}_7$	0.5	0.1816	0.1148	0.8402
34	$\text{Sm}_2\text{Zr}_2\text{O}_7$	0	/	/	0
35	$(\text{Sm}_{0.9}\text{Gd}_{0.1})_2\text{Zr}_2\text{O}_7$	0.1	0.0457	0.0139	0.0026
36	$(\text{Sm}_{0.7}\text{Gd}_{0.3})_2\text{Zr}_2\text{O}_7$	0.3	0.0453	0.0139	0.0079
37	$(\text{Sm}_{0.5}\text{Gd}_{0.5})_2\text{Zr}_2\text{O}_7$	0.5	0.0449	0.0140	0.0133
38	$(\text{Sm}_{0.9}\text{Gd}_{0.05}\text{Yb}_{0.05})_2\text{Zr}_2\text{O}_7$	0.05+0.05	0.0454+0.1488	0.0140+0.0884	0.0674
39	$(\text{Sm}_{5/6}\text{Yb}_{1/6})_2\text{Zr}_2\text{O}_7$	1/6	0.1466	0.0893	0.1701
40	$(\text{Sm}_{2/3}\text{Yb}_{1/3})_2\text{Zr}_2\text{O}_7$	1/3	0.1431	0.0906	0.3485
41	$(\text{Sm}_{1/2}\text{Yb}_{1/2})_2\text{Zr}_2\text{O}_7$	1/2	0.1398	0.0920	0.5388
42	$\text{Gd}_2\text{Zr}_2\text{O}_7$	0	/	/	0
43	$(\text{Gd}_{0.98}\text{Yb}_{0.02})_2\text{Zr}_2\text{O}_7$	0.02	0.0996	0.0752	0.0143
44	$(\text{Gd}_{0.96}\text{Yb}_{0.04})_2\text{Zr}_2\text{O}_7$	0.04	0.0994	0.0753	0.0288
45	$(\text{Gd}_{0.94}\text{Yb}_{0.06})_2\text{Zr}_2\text{O}_7$	0.06	0.0992	0.0755	0.0433
46	$(\text{Gd}_{0.92}\text{Yb}_{0.08})_2\text{Zr}_2\text{O}_7$	0.08	0.0990	0.0756	0.0579
47	$(\text{Gd}_{0.90}\text{Yb}_{0.10})_2\text{Zr}_2\text{O}_7$	0.10	0.0988	0.0757	0.0726
48	$\text{Gd}_2(\text{Zr}_{0.9}\text{Ti}_{0.1})_2\text{O}_7$	0.1	0.4984	0.1695	0.3840
49	$\text{Gd}_2(\text{Zr}_{0.8}\text{Ti}_{0.2})_2\text{O}_7$	0.2	0.5246	0.1724	0.7981
50	$\text{Gd}_2(\text{Zr}_{0.7}\text{Ti}_{0.3})_2\text{O}_7$	0.3	0.5536	0.1754	1.2456
51	$\text{Gd}_2(\text{Zr}_{0.6}\text{Ti}_{0.4})_2\text{O}_7$	0.4	0.5861	0.1756	1.6792
52	$\text{Gd}_2(\text{Zr}_{0.5}\text{Ti}_{0.5})_2\text{O}_7$	0.5	0.6226	0.1818	2.2595

ically shown in Fig. 9(c), Yb^{3+} substitutions with heavier atomic mass and smaller ionic radius are placed in an oversized anion cage in the $\text{La}_2\text{Zr}_2\text{O}_7$ lattice. Their large thermal vibration amplitude acts as a “rattler”, which has been proven to be not only effective in scattering the short-wavelength phonons, but also important in limiting the mid-to-long wavelength ones. Therefore, $(\text{La}_{1-x}\text{Yb}_x)_2\text{Zr}_2\text{O}_7$ materials have an extremely low thermal conductivity approaching the theoretical minimum value. Similar phenomena are also reported in $(\text{La}_{1-x}\text{Er}_x)_2\text{Zr}_2\text{O}_7$ and some other materials [68]. However, fundamental understanding and quantitative estimation of these phenomena are still lacking.

As indicated in Eqs. (9) and (10), the thermal conductivity of defective materials is approximately inversely proportional to the square root of the phonon scattering coefficient. Therefore, we can plot the relation between the $1/\Gamma^{0.5}$ and κ to estimate the validity of the point defect phonon scattering model. As summarized in Fig. 14, thermal conductivities of the substituted materials listed in Tables 4 and 5 at 200 °C are mainly within a linearly increasing

zone with $1/\Gamma^{0.5}$, which corresponds to the point defect phonon scattering model. It should be clarified that the thermal conductivities of them are given as the ratio of the substituted material and the “perfect crystal material” for better comparison. The discreteness of the data is probably attributed to the variation of the density and elastic properties of different matrix materials and also to the experimental uncertainties. On the other hand, there are still some materials with small phonon scattering coefficient but unexpectedly low thermal conductivity, corresponding to the data at the right bottom corner, out of the linearly increasing zone of the point defect phonon scattering model. The unconventional lattice distortions caused by the lattice defects, such as the order-disorder phase transformation or “rattling phenomena”, are the dominant reasons for the thermal conductivity approaching the minimum. Yet, the synergistic effect of the oxygen vacancies and the substitutions still requires further research.

Except for multicomponent materials based on 7YSZ and $\text{Ln}_2\text{Zr}_2\text{O}_7$, substitutions have also been introduced in some other

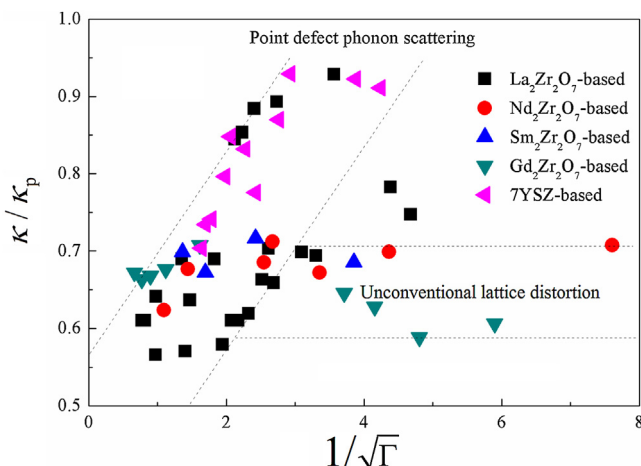


Fig. 14. For most of the materials with equivalent substitutions, the normalized thermal conductivity have an approximately linear relation with $1/\sqrt{\Gamma}$, which corresponds to the point defect phonon scattering model. The abnormal results of the thermal conductivity are mainly dominated by the lattice distortions.

materials to decrease their thermal conductivity, for example in $\text{Zr}_3\text{Y}_4\text{O}_{12}$. Thermal conductivity of the equimolar substituted compound $(\text{Zr}_{0.5}\text{Hf}_{0.5})_3\text{Y}_4\text{O}_{12}$ is about 20% lower than that of δ phase $\text{Zr}_3\text{Y}_4\text{O}_{12}$ [15]. Since the ionic radii of Zr^{4+} and Hf^{4+} are almost the same, the phonon scattering is mainly caused by the mass difference, which can be considered the “isotope effect” as a simplification of the point defect phonon scattering model. Another example is the triply co-substituted $\text{LnMA}_{11}\text{O}_{19}$ ceramics with a thermal conductivity approaching the theoretical minimum [77].

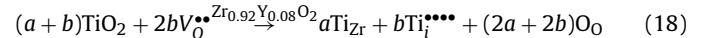
5. Interstitials

In contrast to vacancies and substitutional ions, interstitials should be considered as lattice defects belonging to their own sub-lattice rather than the host lattice. Therefore, the point defect phonon scattering model is no longer appropriate for them. Actually, interstitials have a similar phonon scattering efficiency to that of vacancies [78], but interstitials can hardly be the dominating type of lattice defects in ceramic materials since the concentration of them is usually much lower than that of vacancies or substitutional ions. Therefore, interstitials have little effect on the phonon mean free path in common ceramic materials. On the contrary, they may excite new phonon branches of the whole lattice, which lead to a slightly increase of the heat capacity as well as the thermal conductivity. An example is that in the apatite gadolinium calcium silicates discussed above. Oxygen interstitials are probably the major lattice defects in $\text{Gd}_{10}(\text{SiO}_4)_6\text{O}_3$ and its thermal conductivity is slightly higher than that of the stoichiometric material $\text{Gd}_8\text{Ca}_2(\text{SiO}_4)_6\text{O}_2$ without “intrinsic lattice defects” [56]. However, no direct evidence has been observed to confirm the existence of the oxygen interstitials. So it is difficult to discuss their effect in detail.

On the other hand, cation interstitials have been reported without question and their influence on the thermal conductivity has also been discussed. For example, Qu etc. have investigated the lattice structure and thermal conductivity of $(\text{Sm}_{2-x}\text{Mg}_x)\text{Zr}_2\text{O}_{7-x/2}$ materials [79]. Cation interstitials are the dominant defects when $0 < x < 0.075$ and after that Mg^{2+} substitutions of Sm^{3+} start to take place. This has been confirmed by XRD, Raman, XPS as well as the lattice parameter and density variations of the materials with x . The defect equation of the Mg^{2+} interstitials can be expressed as:



Except for the interstitials (Mg_i^{***}), vacancy reoccupation to maintain neutrality also reduces the concentration of the intrinsic oxygen vacancies in $\text{Sm}_2\text{Zr}_2\text{O}_7$, which has a significant effect on the thermal conductivity increase. The thermal conductivities of all the MgO -doped materials are higher than that of $\text{Sm}_2\text{Zr}_2\text{O}_7$, confirming the effect of interstitials. A similar result has also been reported by Zhao etc. in TiO_2 -doped 7YSZ with a high concentration of Ti^{4+} substitutions. Ti^{4+} interstitials coexist with the Ti^{4+} substitutions of Zr^{4+} as:



where a and b are related to the doping content. Ti^{4+} interstitials are proven by the lattice parameter when the doping content is more than 8% and their concentration is measured by a specially designed method on TEM with EDS accessory. The effect of the interstitials on the thermal conductivity has been semi-quantitatively discussed by a modified point defect phonon scattering model in consideration of both interstitials and oxygen vacancy reoccupations [60].

From the discussions above, perhaps interstitials should be avoided in TBC materials in order to achieve low thermal conductivity. However, it has been reported that the thermal expansion coefficient can be significantly enhanced by cation interstitials, which is also important for the performance of TBC [79]. This is beyond the scope of the present review.

6. Remarks and outlook

In summary, defect engineering has always been a promising and effective method in reducing the thermal conductivity of TBC materials during the last several decades. Among the various kinds of lattice defects, oxygen vacancies seems to be the most efficient in phonon scattering and thermal conductivity reduction. However, a high concentration of oxygen vacancies will facilitate the oxygen diffusion in the oxides, which is undesirable in TBCs to avoid the generation of TGO. Besides, substitutions provide another route for phonon scattering and thermal conductivity reduction. Aliovalent substitutions may generate more oxygen vacancies while equivalent substitutions are also effective when the atomic mass and ionic radius mismatch between the substitution and the host cation is considerable. Interstitials may provide an opposite effect on the thermal conductivity, which should probably be avoided. The thermal conductivity of multicomponent solid solutions based on 7YSZ or $\text{Ln}_2\text{Zr}_2\text{O}_7$ are generally show an inverse proportionality to the square root of the phonon scattering coefficient, which obeys the point defect phonon scattering model.

Defect engineering will definitely remain an effective strategy to develop the next generation of TBC materials with low thermal conductivity and good comprehensive mechanical properties. Unusual lattice defects, which lead to strong lattice distortion and phonon scattering, will be the central theme of defect engineering from now on, demanding more investigation and better understanding in the future.

Acknowledgements

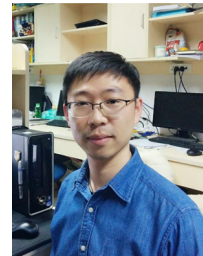
The authors gratefully acknowledge the financial support from National Natural Science Foundation of China (No. 51272120, 51472135, 51072088 and 51590893). Some unpublished results were provided by Dr. Jing Feng. The authors also personally acknowledge his help.

References

- [1] N.P. Padture, M. Gell, E.H. Jordan, Thermal barrier coatings for gas-turbine engine applications, *Science* 296 (2002) 280–284.

- [2] D.R. Clarke, M. Oechsner, N.P. Padture, Thermal-barrier coatings for more efficient gas-turbine engines, *MRS Bull.* 37 (2012) 891–898.
- [3] D.R. Clarke, C.G. Levi, Materials design for the next generation thermal barrier coatings, *Ann. Rev. Mater. Res.* 33 (2003) 383–417.
- [4] N. Curry, N. Markocsan, X.-H. Li, A. Tricoire, M. Dorfman, Next generation thermal barrier coatings for the gas turbine industry, *J. Therm. Spray Technol.* 20 (2010) 108–115.
- [5] S. Sampath, U. Schulz, M.O. Jarligo, S. Kuroda, Processing science of advanced thermal-barrier systems, *MRS Bull.* 37 (2012) 903–910.
- [6] R.S. Lima, B.R. Marple, Thermal spray coatings engineered from nanostructured ceramic agglomerated powders for structural, thermal barrier and biomedical applications: a review, *J. Therm. Spray Technol.* 16 (2007) 40–63.
- [7] C.G. Levi, Emerging materials and processes for thermal barrier systems, *Curr. Opin. Solid State Mater. Sci.* 8 (2004) 77–91.
- [8] A. Feuerstein, J. Knapp, T. Taylor, A. Ashary, A. Bolcavage, N. Hitchman, Technical and economical aspects of current thermal barrier coating systems for gas turbine engines by thermal spray and EBPVD: a review, *J. Therm. Spray Technol.* 17 (2008) 199–213.
- [9] A.G. Evans, D.R. Clarke, J.R. Williams, C. Mercer, On a ferroelastic mechanism governing the toughness of metastable tetragonal-prime (t') yttria-stabilized zirconia, *Proc. R. Soc. Lond. A Mater.* 463 (2007) 1393–1408.
- [10] J. Chevalier, L. Gremillard, A.V. Virkar, D.R. Clarke, The tetragonal-monoclinic transformation in zirconia: lessons learned and future trends, *J. Am. Ceram. Soc.* 92 (2009) 1901–1920.
- [11] R. Vassen, X.Q. Cao, F. Tietz, D. Basu, D. Stover, Zirconates as new materials for thermal barrier coatings, *J. Am. Ceram. Soc.* 83 (2000) 2023–2028.
- [12] J. Wu, X.Z. Wei, N.P. Padture, P.G. Klemens, M. Gell, E. Garcia, P. Miranzo, M.I. Osendi, Low thermal conductivity rare earth zirconates for potential thermal barrier coating applications, *J. Am. Ceram. Soc.* 85 (2002) 3031–3035.
- [13] J. Feng, B. Xiao, R. Zhou, W. Pan, Thermal conductivity of rare earth zirconate pyrochlore from first principles, *Scripta Mater.* 68 (2013) 727–730.
- [14] D.R. Clarke, S.R. Phillipot, Thermal barrier coating materials, *Mater. Today* 8 (2005) 22–29.
- [15] M.R. Winter, D.R. Clarke, Oxide materials with low thermal conductivity, *J. Am. Ceram. Soc.* 90 (2007) 533–540.
- [16] X.Q. Cao, R. Vassen, D. Stoever, Ceramic materials for thermal barrier coatings, *J. Eur. Ceram. Soc.* 24 (2004) 1–10.
- [17] W. Pan, S.R. Phillipot, C. Wan, A. Chernatynskiy, Z. Qu, Low thermal conductivity oxides, *MRS Bull.* 37 (2012) 917–922.
- [18] W. Ma, D.E. Mack, R. Vařen, D. Stöver, Perovskite-type strontium zirconate as a new material for thermal barrier coatings, *J. Am. Ceram. Soc.* 91 (2008) 2630–2635.
- [19] R. Wu, W. Pan, X. Ren, C. Wan, Z. Qu, A. Du, An extremely low thermal conduction ceramic: $\text{RE}_{0.93}(\text{SiO}_4)_6\text{O}_2$ silicate oxyapatite, *Acta Mater.* 60 (2012) 5536–5544.
- [20] X. Chen, L. Gu, B. Zou, Y. Wang, X. Cao, New functionally graded thermal barrier coating system based on $\text{LaMgAl}_{11}\text{O}_{19}/\text{YSZ}$ prepared by air plasma spraying, *Surf. Coat. Tech.* 206 (2012) 2265–2274.
- [21] G. Grimvall, *Thermophysical Properties of Materials*, ELSEVIER, Amsterdam, 1999.
- [22] W.D. Kingery, H.K. Bowen, D.R. Uhlmann, *Introduction to Ceramics*, John Wiley & Sons Inc, NewYork, 1960.
- [23] M.G. Holland, Analysis of lattice thermal conductivity, *Phys. Rev.* 132 (1963) 2461–2471.
- [24] J. Callaway, Model for lattice thermal conductivity at low temperatures, *Phys. Rev.* 113 (1959) 1046–1051.
- [25] B. Abeles, Lattice thermal conductivity of disordered semiconductor alloys at high temperatures, *Phys. Rev.* 131 (1963) 1906–1911.
- [26] P.G. Klemens, Thermal resistance due to point defects at high temperatures, *Phys. Rev.* 119 (1960) 507–509.
- [27] J. Callaway, H.C. von Baeyer, Effect of point imperfections on lattice thermal conductivity, *Phys. Rev.* 120 (1960) 1149–1154.
- [28] R.E. Nettleton, Foundations of the callaway theory of thermal conductivity, *Phys. Rev.* 132 (1963) 2032–2038.
- [29] C.L. Wan, W. Pan, Q. Xu, Y.X. Qin, J.D. Wang, Z.X. Qu, M.H. Fang, Effect of point defects on the thermal transport properties of $(\text{La},\text{Gd}_{1-x})_2\text{Zr}_2\text{O}_7$: experiment and theoretical model, *Phys. Rev. B* 74 (44109) (2006) 9.
- [30] D.G. Cahill, S.K. Watson, R.O. Pohl, Lower limit to the thermal conductivity of disordered crystals, *Phys. Rev. B* 46 (1992) 6131–6140.
- [31] M.P. Zaitlin, A.C. Anderson, Phonon thermal transport in noncrystalline materials, *Phys. Rev. B* 12 (1975) 4475–4486.
- [32] H.G. Scott, Phase relationships in the yttria-rich part of the yttria-zirconia system, *J. Mater. Sci.* 12 (1977) 311–316.
- [33] Y. Du, Z. Jin, P. Huang, Thermodynamic assessment of the $\text{ZrO}_2\text{-YO}_{1.5}$ system, *J. Am. Ceram. Soc.* 74 (1991) 1569–1577.
- [34] T.A. Schaedler, R.M. Leckie, S. Krämer, A.G. Evans, C.G. Levi, Toughening of nontransformable t' -YSZ by addition of titania, *J. Am. Ceram. Soc.* 90 (2007) 3896–3901.
- [35] X. Cao, Application of rare earths in thermal barrier coating materials, *J. Mater. Sci. Technol.* 23 (2007) 15–35.
- [36] L. Guo, H. Guo, S. Gong, H. Xu, Improvement on the phase stability, mechanical properties and thermal insulation of Y_2O_3 -stabilized ZrO_2 by Gd_2O_3 and Yb_2O_3 co-doping, *Ceram. Int.* 39 (2013) 9009–9015.
- [37] L. Guo, M. Li, F. Ye, Phase stability and thermal conductivity of RE_2O_3 ($\text{RE} = \text{La, Nd, Gd, Yb}$) and Yb_2O_3 co-doped Y_2O_3 stabilized ZrO_2 ceramics, *Ceram. Int.* 42 (2016) 7360–7365.
- [38] X. Song, M. Xie, X. Hao, G. Jia, S. An, Structure and thermal conductivity of $\text{Zr}_{1-x}\text{Gd}_x\text{O}_{2-x/2}$ solid solutions, *J. Alloy Compd.* 497 (2010) L5–L8.
- [39] L. Sun, H. Guo, H. Peng, S. Gong, H. Xu, Influence of partial substitution of Sc_2O_3 with Gd_2O_3 on the phase stability and thermal conductivity of Sc_2O_3 -doped ZrO_2 , *Ceram. Int.* 39 (2013) 3447–3451.
- [40] L. Sun, H. Guo, H. Peng, S. Gong, H. Xu, Phase stability and thermal conductivity of ytterbia and yttria co-doped zirconia, *Prog. Nat. Sci.* 23 (2013) 440–445.
- [41] Z.X. Qu, *Defect Chemistry and Thermophysical Properties of Rare-Earth Oxide Ceramics for Thermal Barrier Coating Applications*. PhD Thesis, Tsinghua University, 2009.
- [42] Z.-G. Liu, J.-H. Ouyang, B.-H. Wang, Y. Zhou, J. Li, Thermal expansion and thermal conductivity of $\text{Sm}_x\text{Zr}_{1-x}\text{O}_{2-x/2}$ ($0.1 \leq x \leq 0.5$) ceramics, *Ceram. Int.* 35 (2009) 791–796.
- [43] L. Guo, Y. Zhang, F. Ye, M.A. White, Phase structure evolution and thermo-physical properties of nonstoichiometry $\text{Nd}_{2-x}\text{Zr}_{2+x}\text{O}_{7+x/2}$ pyrochlore ceramics, *J. Am. Ceram. Soc.* 98 (2015) 1013–1018.
- [44] J.-F. Bisson, Thermal conductivity of yttria-zirconia single crystals, determined with spatially resolved infrared thermography, *J. Am. Ceram. Soc.* 83 (2000) 1993–1998.
- [45] P.K. Schelling, S.R. Phillipot, R.W. Grimes, Optimum pyrochlore compositions for low thermal conductivity, *Phil. Mag. Lett.* 84 (2004) 127–137.
- [46] M.A. Subramanian, A.G. Aravamudan, G.V.S. Rao, Oxide pyrochlores—a review, *Prog. Solid State Chem.* 15 (1983) 55–143.
- [47] A.R. Cleave, Atomic scale simulation for waster form application. PhD thesis, Imperial College of Science, Technol. Med. (2006).
- [48] Z.-G. Liu, J.-H. Ouyang, Y. Zhou, Preparation and thermophysical properties of $(\text{Nd}_x\text{Gd}_{1-x})_2\text{Zr}_2\text{O}_7$ ceramics, *J. Mater. Sci.* 43 (2008) 3596–3603.
- [49] Z.-G. Liu, J.-H. Ouyang, Y. Zhou, Structural evolution and thermophysical properties of $(\text{Sm}_x\text{Gd}_{1-x})_2\text{Zr}_2\text{O}_7$ ($0 \leq x \leq 1.0$) ceramics, *J. Alloy Compd.* 472 (2009) 319–324.
- [50] C. Wan, Z. Qu, A. Du, W. Pan, Order-Disorder transition and unconventional thermal conductivities of the $(\text{Sm}_{1-x}\text{Yb}_x)_2\text{Zr}_2\text{O}_7$ series, *J. Am. Ceram. Soc.* 94 (2011) 592–596.
- [51] M. Zhao, Effect of Defects on the Thermophysical Properties of Zirconia-Based Thermal Barrier Coating Materials PhD Thesis, Tsinghua University, 2016.
- [52] L.M. Kovba, E.V. Lykova Ln Antipov, M.G. Rozova, $\text{BaO-Ln}_2\text{O}_3\text{-Al}_2\text{O}_3$ systems, *Russ. J. Inorg. Chem. (Engl. Transl.)* 29 (1984) 3137–3142.
- [53] C. Wan, Z. Qu, Y. He, D. Luan, W. Pan, Ultralow thermal conductivity in highly anion-defective aluminates, *Phys. Rev. Lett.* 101 (085901) (2008) 4pp.
- [54] J. Feng, Unpublished result of thermal conductivity of $\text{Ba}_6\text{Ln}_2\text{Al}_4$ 2016 O₁₅.
- [55] A.V. Teterskii, S.Y. Stefanovich, N.Y. Turova, Sol-gel synthesis of oxygen-ion conductors based on apatite-structure silicates and silicophosphates, *Inorg. Mater.* 42 (2006) 294–302.
- [56] Z. Qu, T.D. Sparks, W. Pan, D.R. Clarke, Thermal conductivity of the gadolinium calcium silicate apatites: effect of different point defect types, *Acta Mater.* 59 (2011) 3841–3850.
- [57] M. Martena, D. Botto, P. Fino, S. Sabbadini, M.M. Gola, C. Badini, Modelling of TBC system failure: stress distribution as a function of TGO thickness and thermal expansion mismatch, *Eng. Fail. Anal.* 13 (2006) 409–426.
- [58] J. Wu, N.P. Padture, P.G. Klemens, M. Gell, E. Garcia, P. Miranzo, M.I. Osendi, Thermal conductivity of ceramics in the $\text{ZrO}_2\text{-GdO}_{1.5}$ system, *J. Mater. Res.* 17 (2002) 3193–3200.
- [59] J. Feng, X. Ren, X. Wang, R. Zhou, W. Pan, Thermal conductivity of ytterbia-stabilized zirconia, *Scripta Mater.* 66 (2012) 41–44.
- [60] M. Zhao, W. Pan, Effect of lattice defects on thermal conductivity of Ti-doped, Y_2O_3 -stabilized ZrO_2 , *Acta Mater.* 61 (2013) 5496–5503.
- [61] M. Zhao, X. Ren, W. Pan, J. Smialek, Low thermal conductivity of SnO_2 -doped Y_2O_3 -stabilized ZrO_2 : effect of the lattice tetragonal distortion, *J. Am. Ceram. Soc.* 98 (2015) 229–235.
- [62] M. Zhao, X. Ren, J. Yang, W. Pan, Thermo-mechanical properties of ThO_2 -doped Y_2O_3 stabilized ZrO_2 for thermal barrier coatings, *Ceram. Int.* 42 (2016) 501–508.
- [63] M. Zhao, X. Ren, W. Pan, Effect of lattice distortion and disordering on the mechanical properties of titania-doped yttria-stabilized zirconia, *J. Am. Ceram. Soc.* 97 (2014) 1566–1571.
- [64] R.D. Shannon, Revised effective ionic radii and systematic studies of interatomic distances in halides and chalcogenides, *Acta Crystallogr. A* 32 (1976) 751–767.
- [65] Y. Shen, R.M. Leckie, C.G. Levi, D.R. Clarke, Low thermal conductivity without oxygen vacancies in equimolar $\text{YO}_{1.5} + \text{TaO}_{2.5}$ and $\text{YbO}_{1.5} + \text{TaO}_{2.5}$ -stabilized tetragonal zirconia ceramics, *Acta Mater.* 58 (2010) 4424–4431.
- [66] X. Song, M. Xie, R. Mu, F. Zhou, G. Jia, S. An, Influence of the partial substitution of Y_2O_3 with Ln_2O_3 ($\text{Ln} = \text{Nd, Sm, Gd}$) on the phase structure and thermophysical properties of $\text{ZrO}_2\text{-Nb}_2\text{O}_5\text{-Y}_2\text{O}_3$ ceramics, *Acta Mater.* 59 (2011) 3895–3902.
- [67] D.M. Zhu, R.A. Miller, Development of Advanced Low Conductivity Thermal Barrier Coatings. NASA/TM-2004-212961.
- [68] Y. Zhang, M. Xie, F. Zhou, X. Cui, X. Lei, X. Song, S. An, Influence of Er substitution for La on the thermal conductivity of $(\text{La}_{1(1-x)}\text{Er}_x)_2\text{Zr}_2\text{O}_7$ pyrochlores, *Mater. Res. Bull.* 64 (2015) 175–181.
- [69] X. Wang, L. Guo, H. Zhang, S. Gong, H. Guo, Structural evolution and thermal conductivities of $(\text{Gd}_{1-x}\text{Yb}_x)_2\text{Zr}_2\text{O}_7$ ($x = 0, 0.02, 0.04, 0.06, 0.08, 0.1$) ceramics for thermal barrier coatings, *Ceram. Int.* 41 (2015) 12621–12625.

- [70] Y. Zhang, M. Xie, F. Zhou, X. Cui, X. Lei, X. Song, S. An, Low thermal conductivity in $\text{La}_2\text{Zr}_2\text{O}_7$ pyrochlore with A-site partially substituted with equimolar Yb_2O_3 and Er_2O_3 , *Ceram. Int.* 40 (2014) 9151–9157.
- [71] Y. Wang, F. Yang, P. Xiao, Role and determining factor of substitutional defects on thermal conductivity: a study of $\text{La}_2(\text{Zr}_{1-x}\text{B}_x)_2\text{O}_7$ ($\text{B}=\text{Hf}, \text{Ce}, 0 \leq x \leq 0.5$) pyrochlore solid solutions, *Acta Mater.* 68 (2014) 106–115.
- [72] C. Wan, W. Zhang, Y. Wang, Z. Qu, A. Du, R. Wu, W. Pan, Glass-like thermal conductivity in ytterbium-doped lanthanum zirconate pyrochlore, *Acta Mater.* 58 (2010) 6166–6172.
- [73] H. Zhang, K. Sun, Q. Xu, F. Wang, L. Liu, Thermal conductivity of $(\text{Sm}_{1-x}\text{La}_x)_2\text{Zr}_2\text{O}_7$ ($x=0, 0.25, 0.5, 0.75$ and 1) oxides for advanced thermal barrier coatings, *J. Rare Earth* 27 (2009) 222–226.
- [74] C. Wan, Z. Qu, A. Du, W. Pan, Influence of B site substituent Ti on the structure and thermophysical properties of $\text{A}_2\text{B}_2\text{O}_7$ -type pyrochlore $\text{Gd}_2\text{Zr}_2\text{O}_7$, *Acta Mater.* 57 (2009) 4782–4789.
- [75] Z.G. Liu, J.H. Ouyang, Y. Zhou, Q.C. Meng, X.L. Xia, Order-disorder transition and thermal conductivity of $(\text{Yb}_x\text{Nd}_{1-x})_2\text{Zr}_2\text{O}_7$ solid solutions, *Philos. Mag.* 89 (2009) 553–564.
- [76] M. Zhao, X. Ren, J. Yang, W. Pan, Low thermal conductivity of rare-earth zirconate-stannate solid solutions $(\text{Yb}_2\text{Zr}_2\text{O}_7)_{1-x}(\text{Ln}_2\text{Sn}_2\text{O}_7)_x$ ($\text{Ln}=\text{Nd}, \text{Sm}$), *J. Am. Ceram. Soc.* 99 (2016) 293–299.
- [77] H. Lu, C.-A. Wang, Y. Huang, H. Xie, Multi-enhanced-phonon scattering modes in In-Me-A sites co-substituted $\text{LnMeAl}_1\text{O}_{19}$ ceramics, *Sci. Rep.* 4 (6823) (2014) 7.
- [78] L.L. Snead, S.J. Zinkle, D.P. White, Thermal conductivity degradation of ceramic materials due to low temperature, low dose neutron irradiation, *J. Nucl. Mater.* 340 (2005) 187–202.
- [79] Z.X. Qu, C.L. Wan, W. Pan, Thermal expansion and defect chemistry of mgO -doped $\text{Sm}_2\text{Zr}_2\text{O}_7$, *Chem. Mater.* 19 (2007) 4913–4918.



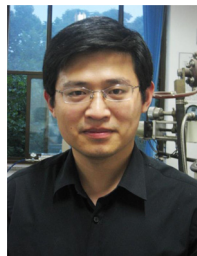
Meng Zhao State Key-Lab of New Ceramics and Fine Processing, School of Materials Science and Engineering, Tsinghua University, Beijing 100084, China. Zhao is a PhD candidate in the School of Materials Science and Engineering, Tsinghua University. He received his bachelor degree in materials science and engineering in 2011 from Tsinghua University. His research focuses on low thermal conductivity materials for thermal barrier coatings.



Wei Pan State Key-Lab of New Ceramics and Fine Processing, School of Materials Science and Engineering, Tsinghua University, Beijing 100084, China. Pan is the professor and director of State Key Lab of New Ceramics and Fine Processing, Tsinghua University. He received his BS (1982) degree in engineering from the University of Science and Technology Beijing in China, MS (1987) and PhD (1990) degrees in engineering from Nagoya University in Japan. He currently serves as a member of the University Council of Tsinghua University; fellow of the School of Engineering of the University of Tokyo; member of the standing-committee of the Chinese Ceramic Society, and member of the editorial board of several international journals. He is also the academician of the World Academy of Ceramics. His research interests include low thermal conductivity ceramics for gas-turbines, solid-electrolytes and nanomaterials.



Chunlei Wan State Key-Lab of New Ceramics and Fine Processing, School of Materials Science and Engineering, Tsinghua University, Beijing 100084, China. Wan is an assistant professor in the State Key-Lab of New Ceramics and Fine Processing, School of Materials Science and Engineering, Tsinghua University. He received his PhD degree in materials science and engineering (2008) from Tsinghua University. During 2008.10~2015.5, Wan worked as assistant professor in Nagoya University. His research interests include thermal barrier coating materials, thermoelectric materials, and phonon and electron transport phenomena in solid state materials.



Zhixue Qu College of Materials Science and Engineering, Beijing University of Technology, Beijing 100124, China. Qu is an assistant professor in the College of Materials Science and Engineering, Beijing University of Technology in China. He received his PhD in materials science and engineering from Tsinghua University (2009). His research interests include the defect chemistry and thermophysical properties of materials as well as the synthesis and characterization of electromagnetic materials. He has authored or co-authored more than 20 publications in these fields.



Zheng Li State Key-Lab of New Ceramics and Fine Processing, School of Materials Science and Engineering, Tsinghua University, Beijing 100084, China. Li is a PhD candidate in School of Materials Science and Engineering, Tsinghua University. He received his bachelor degree in material science in 2013 from Fudan University. His research interests include the heat conduction in solid state materials and superconducting materials.



Jun Yang State Key-Lab of New Ceramics and Fine Processing, School of Materials Science and Engineering, Tsinghua University, Beijing 100084, China. Yang is a PhD candidate in the School of Materials Science and Engineering, Tsinghua University. His research focuses on the investigation of thermophysical properties of solid state materials by first-principles calculation.